THESIS FOR THE DEGREE OF LICENTIATE OF ENGINEERING IN PHYSICS

Partial methane oxidation from electronic structure calculations

ADAM A. ARVIDSSON

CHALMERS

Partial methane oxidation from electronic structure calculations
ADAM A. ARVIDSSON

Cover:
The $[\text{Cu-O-Cu}]^{2+}$ motif in ZSM-5 zeolite that can convert methane to methanol.

Partial methane oxidation from electronic structure calculations
Thesis for the degree of Licentiate of Engineering in Physics
ADAM A. ARVIDSSON
Department of Physics
Division of Chemical Physics
Chalmers University of Technology

Abstract

Investigating catalytic reactions with computational methods is a powerful approach to understand fundamental aspects of catalytic reactions and find ways to guide catalytic design. Partial methane oxidation is one example of a reaction with intriguing challenges, where a detailed atomistic approach may help to unravel the bottlenecks of this, as of yet, inefficient reaction. Although methane only needs one oxygen atom for conversion to methanol, the direct oxidation is difficult; it is in fact so difficult that at many oil extraction sites, the methane that inevitably accompanies the crude oil is flared into carbon dioxide and water as gas-phase methane is too inconvenient to store and transport.

The main challenge with partial oxidation of methane is to selectively control the oxidation and steer it towards methanol and prevent over-oxidation to CO_2. There exist natural enzymes that can partially oxidize methane to methanol at ambient pressure and temperature, although very slowly. One inorganic analogue to these naturally occurring enzymes are zeolites, a porous material that can readily be synthesized and that have been shown to convert methane to methanol at ambient conditions with a high selectivity (>90 %). This has been realized for zeolites ion-exchanged with different metals, such as iron, cobalt, nickel, and copper. Although there have been many attempts to determine the active site for the reaction, there is still no consensus. One candidate that has been put forth is a $[Cu-O-Cu]^{2+}$ motif experimentally characterized in the ZSM-5 zeolite. In this thesis, partial oxidation of methane is investigated, focusing on this dimer motif. By combining density functional theory calculations with microkinetic modelling, the catalytic performance of the dimer motif is investigated with a simple reaction mechanism for copper, but also with the copper atoms exchanged with nickel, cobalt, iron, silver, or gold. From these results, it is clear that this particular dimer site is a relevant candidate only for copper, and can be excluded in the continued search for active sites in nickel, cobalt, and iron ion-exchanged ZSM-5.

To further understand how methanol is formed and interacts with Cu-ZSM-5, experimental and calculated infrared frequencies are compared for methanol and other adsorbates. The partial oxidation of methane is also studied for other systems with oxidants other than oxygen. In particular, methane oxidation with H_2S to CH_3SH and H_2 is explored on molybdenum sulfide clusters.

Keywords: partial methane oxidation, density functional theory, microkinetic modelling, ZSM-5 zeolite, Mo_6S_8 cluster

List of Publications

This thesis is based on the following appended papers:

Paper I:

Metal dimer sites in ZSM-5 zeolite for methane-to-methanol conversion from first-principles kinetic modelling: is the $[Cu-O-Cu]^{2+}$ motif relevant for Ni, Co, Fe, Ag, and Au?
Adam A. Arvidsson, Vladimir P. Zhdanov, Per-Anders Carlsson, Henrik Grönbeck, and Anders Hellman
Catal. Sci. Technol., **7** (2017), 1470-1477

Paper II:

Characterization of methanol desorption from Cu-ZSM-5 by *in situ* infrared spectroscopy and first-principles calculations
Xueting Wang, Adam A. Arvidsson, Natalia M. Martin, Johan Nilsson, Stefan Carlson, Johan Gustafson, Magnus Skoglundh, Anders Hellman, and Per-Anders Carlsson
In manuscript

Paper III:

CH_4 and H_2S reforming to CH_3SH and H_2 catalyzed by metal promoted Mo_6S_8 cluster: a first-principles micro-kinetic study
William Taifan, Adam A. Arvidsson, Eric Nelson, Anders Hellman, and Jonas Baltrusaitis
Submitted to Catal. Sci. Technol.

My contributions to the publications

Paper I
I performed all the calculations and wrote the first draft of the paper.

Paper II
I performed all the calculations and co-authored the theoretical part of the manuscript.

Paper III
I performed all microkinetic simulations and co-authored part of the manuscript.

Contents

Chapter 1

Introduction

> ''
> Jag skall derföre, för att begagna en i kemien välkänd härledning, kalla den kroppars *katalytiska kraft*, sönderdelning genom denna kraft *katalys*, likasom vi med ordet analys beteckna åtskiljandet af kroppars beståndsdelar medelst den vanliga kemiska frändeskapen.[1]
>
> – Jöns Jacob Berzelius [1]

When Jöns Jacob Berzelius coined the phrase *catalysis* in 1835 he did it more in order to offer a classification rather than an explanation, in the Linneaus tradition of naming and sorting things [2, 3]. Inspired by experiments by Edmund and Humphry Davy in England, and Döbereiner and Mitscherlich in Germany, Berzelius wanted to classify the observations they had made. While trying to develop a safer lamp for coal miners, Humphry Davy recognized that a platinum wire when exposed to oxygen and coal gas (methane) would glow white hot and was able to keep the wire of the lamp glowing even without a flame. Davy did not understand the phenomenon and described it as "more like magic than anything I have seen" [4–6]. Shortly after, Edmund Davy carried out experiments with platinum powder and observed that it reacted strongly with alcohol vapour at room temperature, remaining hot until all alcohol was consumed. Inspired by Davys' work, Johann Wolfgang Döbereiner noted that platinum also had extraordinary effects on hydrogen oxidation. With pure oxygen, the reaction was so violent that it charred the filter paper holding the platinum powder. However, it was Eilhard Mitscherlich's research on the formation of ether from alcohol when mixed with sulfuric acid that made Berzelius realize that it was the same phenomenon that Davy and Döbereiner had observed with platinum [1]. Berzelius realized that several materials, in solid form or in solution, could exert this influence, which could not be described by standard chemistry at that time. Since these substances seemed to partake in the chemical reactions, without being consumed themselves, Berzelius coined the new concept, *catalysis*, deriving from from the greek words *kata* meaning down, and *lyein* meaning loosen [5], to describe this new phenomenon. These first years of catalysis followed by countless applications and big discoveries and realizations. Our understanding of the field since then has increased tremendously, and with the use of surface science and computational chemistry/physics the aim is to understand catalysis and catalysts all the way down to the atomistic scale.

This thesis focuses on the catalytic direct conversion of methane to methanol, and this first introductory chapter will try to set the stage for the following by motivating

---

[1]Translation: I shall, therefore, to use a well-known derivation in chemistry, call it bodies' catalytic force and the decomposition by this force catalysis, just as we signify by the word analysis the separation of the constituents of bodies by the usual chemical affinities.

the work, give a brief background on the field of catalysis as it developed in the centuries after Berzelius, and define the scope of the thesis.

1.1 Motivation

Why is partial methane oxidation interesting? Methane is the main component of biogas and natural gas, along with smaller amounts of higher alkanes, such as ethane, propane and buthane [7]. The known reserves of natural gas were 190 trillion cubic meters at the end of 2014, which are enough to be able to sustain the global consumption for more than half a century [8]. Unfortunately, much of these reserves are located in isolated areas, like offshore oil wells, and a lot of it is flared into carbon dioxide and water. It is estimated that $3.5\,\%$, or about 143 billion cubic metres, of the natural gas globally extracted was flared in 2012 [9]. Thanks to the low carbon emission per energy unit, natural gas is often considered a good transitional energy source [10, 11]. Furthermore, methane is important as a raw material for other upgraded products [12, 13]. Therefore, methods to convert methane into a liquid, the most simple one being methanol, are highly desirable. These would allow storage at, and transportation from, various extractions sites, making this valuable resource accessible to the chemical industry, and consequently flaring would not be necessary. Being able to liquefy methane in biogas would also increase efficiency and less methane would slip into the atmosphere. However, to be able to do this, partial oxidation of methane is necessary. The alternative, complete oxidation, would give carbon dioxide, which is to put it mildly, less useful.

Currently, industrial conversion of methane into methanol is a two-step process, where synthesis gas, or syngas (CO and H_2) is produced in an intermediate step, which is then converted into methanol or other chemicals [14]. This is very energy-intensive as it requires high pressures and temperatures at large, centralized plants. The alternative, and the outmost aim of this thesis, is to be able to efficiently and directly convert methane to methanol in one step. A challenge that puts catalytic research in the centre.

1.2 Catalysis

To be able to selectively convert methane to, for instance, methanol, a catalyst is needed. A catalyst is a material that accelerates a chemical reaction, which may otherwise be slow or even impossible, but is not consumed itself. The simplest way of looking at this is that the catalyst forms bonds with the reactant, weakens bonds in the reactant, and offers a different pathway that facilitates the reaction, see figure 1.1a.

Catalysis is not a foreign phenomena for most of us, and can be found in every-day examples such as in the aftertreatment system found in almost all vehicles, where catalysts clean the exhaust from, amongst others, poisonous carbon monoxide and nitrogen oxides. In the chemical industry one can find the iron-based catalyst used in the Haber-Bosch process, which enables synthesis of fertilizers that feed the growing global population [17, 18]. These are examples of *heterogeneous catalysis* where the reactants and the catalysts are in different phases, *i.e.* the catalysts are solids and the reactants gases or liquids.

(a) Catalysis

(b) Volcano plot
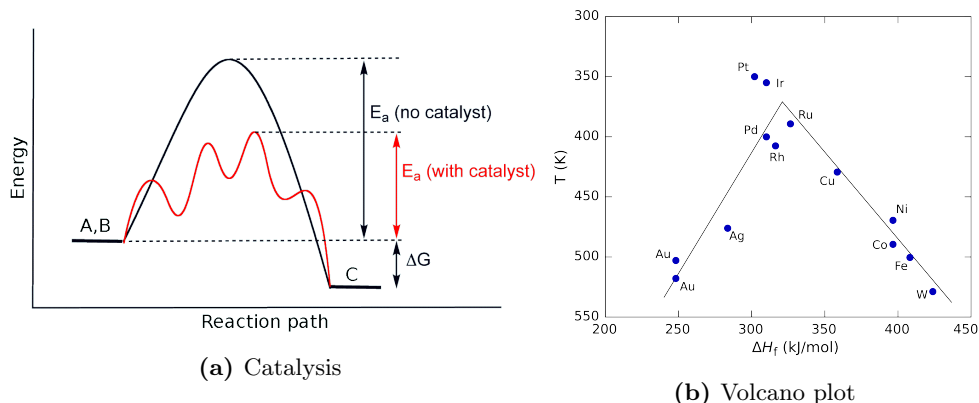
Figure 1.1: Illustration of how a catalyst (a) presents an alternative reaction path to the same product. By binding reactants A and B, intermediate bonds and adsorbates are formed on the catalyst, which can then desorb and form the product C. In (b) an illustration of the Sabatier principle and a volcano plot of the decomposition of formic acid on transition metals. Figure (a) is adapted from, and (b) is taken from Wikimedia Commons [15, 16].

Other classes of catalysis are *homogeneous catalysis*, where both the reactants and the catalyst are in the same phase, often in solution, and *biocatalysis*, with highly efficient enzymes that often use shape selectivity of the substrates or the transition states to catalyze a reaction. Enzymes are a common source of inspiration for the design of catalysts.

According to the Sabatier principle, there is an optimum for a catalytic reaction when the interaction between adsorbates and catalyst is neither too strong, in which case the catalyst is poisoned or deactivated, nor too weak so the reaction never happens[2] [19]. This is often illustrated in a volcano plot where the catalytic activity is plotted against a descriptor of the reaction. One example of this is the decomposition of formic acid on different transition metal catalysts where the heat of formation of the formate salt intermediate, ΔH_f, is used as a descriptor, see figure 1.1b. The temperature at which the reaction reaches a specific rate has an optimum when the interaction with the catalyst is neither to strong, nor to weak. The best performance is obtained for metals in the platinum group when the reaction temperature is lowest. For lower values of ΔH_f, adsorption is slow and limiting, and at higher values the desorption becomes rate-limiting and the catalyst poisoned.

1.3 Zeolites - a porous choice

Zeolites were first described in 1756 by Axel Fredrik Cronstedt [20]. He observed that they produced large amount of steam upon heating and he named them zeolites after the greek

---

[2]This is perfectly expressed with the Swedish word *lagom*.

words *zeo*, meaning *to boil* and *lithos*, meaning *stone*. They are a porous silicon oxide material with a wide range of pore sizes and cages. The active sites in these materials are typically counter ions, which compensate for the net charge created when exchanging some silicon sites with aluminium. Zeolites are one of the few systems that we know can partially oxidize methane. However, they suffer from low yields and a closed catalytic cycle has just recently been reported [21, 22].

The concept *active site*, that specific groups of atoms are responsible for most of the activity on heterogeneous catalyst surfaces, was first put forth in 1925 by Hugh Stott Taylor [23]. This concept is central in catalysis and is crucial for our understanding and the rational design of new catalytic materials. With respect to zeolites and the methane-to-methanol reaction, there is an ongoing discussion concerning the nature of the active site, *i.e.* its structure and composition, and there is yet no clear answer. More background on zeolites, and in particular the ZSM-5 zeolite can be found in chapter 4.

1.4   Scope

The aim of this thesis is to use electronic structure methods and microkinetic modelling to gain further insight into partial methane oxidation. The first and foremost example of this is the direct conversion of methane to methanol in the ZSM-5 zeolite.

To further understand how methanol is formed and interacts with Cu-ZSM-5, vibrational signatures were calculated for methanol and other adsorbates and compared to experimental results. The partial oxidation of methane were also studied for molybdenum sulfide clusters where methane is oxidized with H_2S to CH_3SH and H_2.

The main method in this thesis density functional theory (DFT). The basics of DFT is discussed in chapter 2. The way electronic structure results are connected to experimentally measurable quantities in this thesis is through statistical physics and microkinetic modelling. This is discussed in more detail in chapter 3. The background and a summary of the most important results in the papers this thesis is based on can be found in chapter 4.

Chapter 2

Electronic structure methods

''
The electron is a *theory* we use; it is so useful in understanding the way nature works that we can almost call it real.

– Richard P. Feynman [24]

Richard Feynman raises an important point. All we have in the natural sciences are models of the real world. We should keep that in mind when we discuss scientific results and pay special attention to the approximations we make and the postulates we assume. This is certainly true when working with electronic structure calculations.

In catalysis, electrons are important as they determine bonding and the weakening and strengthening of bonds as the system interacts with its environment. Electronic structure methods are therefore a useful (and almost necessary) tool for unveiling the details of a catalytic reaction. Electronic structure methods are called *first principles* since they are based only on fundamental assumptions, like the Schrödinger equation, and everything is calculated and predicted from these assumptions.

Density functional theory (DFT) is a common tool in computational physics/chemistry. It is a way of calculating the energy of the electronic system given only the electronic density and the principles of quantum mechanics.

2.1 Density functional theory

In the non-relativistic regime, a quantum mechanical system is defined through the time-independent (or stationary) Schrödinger equation [25]

$$\hat{H}\Psi = E\Psi, \tag{2.1}$$

where $\hat{H}$ is the Hamiltonian and it's eigenvalues E are the quantized energy levels of the system. The solution to the Schrödinger equation gives the total wavefunction Ψ of the system, which in principle contains all properties of the system and is essential for a quantum mechanical description of a system. The goal is therefore to find this wavefunction or, perhaps more preferably, the electron density $n(\mathbf{r}) = |\Psi|^2$.

Since we know that the interaction between charged particles is given by the Coulomb interaction, we can write down the Hamiltonian for the many-body system of N electrons

and K nuclei with charge Z_I [26, 27]

$$\hat{H} = -\sum_{i=1}^{N} \frac{\hbar^2}{2m_e} \nabla_i^2 - \sum_{I=1}^{K} \frac{\hbar^2}{2M_I} \nabla_I^2 + \frac{1}{4\pi\epsilon_0} \sum_{i=1}^{N} \sum_{j>i} \frac{e^2}{|\mathbf{r}_i - \mathbf{r}_j|}$$
$$- \frac{1}{4\pi\epsilon_0} \sum_{I=1}^{K} \sum_{i=1}^{N} \frac{Z_I e^2}{|\mathbf{r}_i - \mathbf{R}_I|} + \frac{1}{4\pi\epsilon_0} \sum_{I=1}^{K} \sum_{J>I} \frac{Z_I Z_J e^2}{|\mathbf{R}_I - \mathbf{R}_J|}, \quad (2.2)$$

where m_e is the mass of the electron, M_I the mass of the nuclei, $\mathbf{R}_I$ the position of nuclei I, and $\mathbf{r}_i$ the position of the electron i. This looks rather complicated and, together with the antisymmetry constraint on the total wavefunction, is not straightforward to solve. It turns out that the stationary Schrödinger equation can only be solved analytically for a one-electron system, e.g. the hydrogen atom. So, to be able to continue, certain approximations have to be made. The first approximation one usually applies is the separation of wavefunctions, the Born-Oppenheimer approximation [28], often justified by the fact that the nuclei (ions) are much heavier than the electrons, $M_I >> m_e$. In most cases, this justifies a time-scale separation by considering the electrons to immediately adapt to changes in the positions of the ions[1]. This means that the electronic and ionic system can be treated separately and for the electrons, the ions can be regarded as fixed. We can therefore drop the ionic kinetic energy term and the ion-ion interaction term in the Hamiltonian and only consider the terms involving electrons

$$\hat{H}_{el} = -\sum_{i=1}^{N} \frac{\hbar^2}{2m_e} \nabla_i^2 + \frac{1}{4\pi\epsilon_0} \sum_{i=1}^{N} \sum_{j>i} \frac{e^2}{|\mathbf{r}_i - \mathbf{r}_j|} - \frac{1}{4\pi\epsilon_0} \sum_{I=1}^{K} \sum_{i=1}^{N} \frac{Z_I e^2}{|\mathbf{r}_i - \mathbf{R}_I|}. \quad (2.3)$$

If we denote the interaction of electron i with the ions $V_{ext}(\mathbf{r}_i)$ and use Hartree atomic units ($\hbar = m_e = e = 1/(4\pi\epsilon_0) = 1$), we can write the Hamiltonian as

$$\hat{H}_{el} = -\frac{1}{2} \sum_i \nabla_i^2 + \sum_i \sum_{j>i} \frac{1}{|\mathbf{r}_i - \mathbf{r}_j|} + \sum_i V_{ext}(\mathbf{r}_i). \quad (2.4)$$

In a wavefunction description, this Hamiltonian is still computationally expensive to solve for more than a few electrons [29].

2.1.1 Introducing the electron density

The idea of working with the electron density instead of the wavefunction has been around ever since 1927 when Thomas and Fermi independently introduced the idea [30, 31]. However, that was without actually knowing that it was formally possible to only use the electron density to evaluate the energy of an electronic system. It was not until 1964 when Hohenberg and Kohn [32] proved that the external potential $V_{ext}(\mathbf{r})$ is uniquely determined by the ground state electron density $n_0(\mathbf{r})$ and that the energy can be written as a *functional* of the electron density $n(\mathbf{r}) = |\Psi|^2$, which is minimized by the ground

---

[1] The word "time" is a bit unfortunate here since we deal with the time-*independent* SE, but the short response time of the electrons to a change in the nuclei positions justifies that they are treated separately.

state [33]. In other words, while the Schrödinger equation gives us a way to construct the density from the potential

$$V_{\text{ext}} \rightarrow \Psi \rightarrow n \tag{2.5}$$

Hohenberg and Kohn tell us how to go from the density to the potential, to the wavefunction which describes everything in the system

$$n \rightarrow V_{\text{ext}} \rightarrow \Psi \tag{2.6}$$

Now we know that we can work only with the density, which is much more efficient since the density is only one number for every point in space, while the wavefunction depends on the coordinates of all electrons.

So far we know that it should be possible to consider the electronic many-body problem in terms of the electron density to obtain the ground state energy by using the variational principle and self-consistent iteration. However, to be able to know how to do this we need the work by Kohn and Sham [34].

2.1.2 The Kohn-Sham approach

One year after the Hohenberg-Kohn theorems, Kohn and Sham laid out a method to evaluate the density functional [34]. They made the ansatz of an auxiliary system of independent particles with orbitals ψ_i whose density

$$n(\mathbf{r}) = \sum_{i=1}^{N} |\psi_i(\mathbf{r})|^2, \tag{2.7}$$

is the real density of the system. This allowed them to write the energy functional in a clever way, namely

$$E_{\text{KS}}[n] = T_0[n] + \int n(\mathbf{r}) V_{\text{ext}}[n(\mathbf{r})] \, \mathrm{d}\mathbf{r} + E_{\text{H}}[n] + E_{\text{xc}}[n], \tag{2.8}$$

lumping the difficult many-body effects together, *i.e.* what we miss when we go from the full many-particle wavefunction Ψ to the independent one-particle orbitals ψ_i, and calling it *exchange-correlation* (xc). Part of why this is such a useful way of writing the energy is that the first term, the kinetic energy of the *non*-interacting electrons, is a large part of the energy and is easy to calculate. The second term we recognize as the interaction with the ions (let us from now on call it $E_{\text{ext}}[n]$), and is also simple to calculate. The third term

$$E_{\text{H}}[n] = \frac{1}{2} \int \int \frac{n(\mathbf{r}) n(\mathbf{r}')}{|\mathbf{r} - \mathbf{r}'|} \, \mathrm{d}\mathbf{r} \, \mathrm{d}\mathbf{r}', \tag{2.9}$$

is the Hartree term which is a mean-field approximation, meaning that each electron feels an average effect from all the other electrons, including itself.

By applying the very useful variational principle on the Kohn-Sham energy functional

$$\frac{\delta E_{\text{KS}}}{\delta \psi_i^*(\mathbf{r})} = 0, \tag{2.10}$$

7

we can derive the Kohn-Sham equation for electron i

$$-\frac{1}{2}\nabla^2\psi_i(\mathbf{r}) + \left[V_{\text{ext}}(\mathbf{r}) + \int \frac{n(\mathbf{r}')}{|\mathbf{r}-\mathbf{r}'|}\,\mathrm{d}\mathbf{r}' + \frac{\delta E_{\text{xc}}}{\delta n(\mathbf{r})}\right]\psi_i(\mathbf{r}) = \varepsilon_i\psi_i(\mathbf{r}). \qquad (2.11)$$

This is an eigenvalue problem for the Kohn-Shalm orbitals ψ_i and eigenvalues ε_i. Provided that we have the exact exchange-correlation functional this would give us the true density $n(\mathbf{r})$. It is important to point out that this transformation to an auxiliary system of one-particle orbitals, the Kohn-Sham orbitals ψ_i, is fundamentally different from the description of the many-body Schrödinger equation with the full many-body wavefunction Ψ and is made only to obtain the true density $n(\mathbf{r})$. The Kohn-Sham orbitals ψ_i and energies ε_i are mathematical constructions, and are not related to the "correct" wavefunction and have no strict physical meaning. There are, however, some relations to the the real system. The eigenvalues are for example related to the total energy according to

$$E[n] = \sum_{i=1}^{N}\varepsilon_i - E_{\text{H}}[n] - \int n(\mathbf{r})V_{\text{xc}}[n(\mathbf{r})]\,\mathrm{d}\mathbf{r} + E_{\text{xc}}[n]. \qquad (2.12)$$

Since we calculate the Hartree energy in terms of the total density and we solve the Kohn-Sham equation for electron i, electron i interacts with itself. This is what is known as the *self-interaction error*, and is something we try to correct for in the exchange-correlation functional.

What a DFT implementation basically does is to solve the Kohn-Sham equations, *i.e.* solve the eigenvalue problems in equation (2.11), in a self-consistent way with an approximation to the exchange-correlation. Many implementations also employ methods that simplifies the treatment of the electrons close to the nucleus, the *core electrons*. Various methods to deal with the core states exists, such as using ultrasoft pseudopotentials [35] or the projected augmented wave method [36–38]. Once the energy and density is found for a certain atomic structure, the ground state of the atomic structure can be obtained by moving the atoms along the forces, which are given by the gradient of the energy [39, 40].

2.2 Exchange-correlation functional

The exchange-correlation part of the energy functional contains the many-body features of the electronic system. The exchange originates from the antisymmetry constraint on the total wavefunction and correlation is what remains. The exact exchange-correlation functional E_{xc} is unfortunately not known. There are however a wide range of functionals available using different approximations. These different categories of approximation were described by John Perdew [41] as a Jacob's ladder[2] which reaches from the Hartree world to the heaven of chemical accuracy. As you climb the ladder and obtain better accuracy, also the computational cost increases.

---

[2]A reference to the biblical story of Jacob: *And he dreamed, and behold, there was a ladder set up on the earth, and the top of it reached to heaven; and behold, the angels of God were ascending and descending on it!* – Genesis 28:12

The simplest approximation, and the one originally used by Kohn and Sham, is the the local density approximation (LDA), where the exchange and correlation energy is only dependent on the local density [34], *i.e.*

$$E_{xc}^{LDA} = \int n(\mathbf{r})\epsilon_{xc}[n(\mathbf{r}), \mathbf{r}] \, d\mathbf{r}, \tag{2.13}$$

where ϵ_{xc} is the exchange-correlation energy density of the homogeneous electron gas, which can be calculated with Monte Carlo methods [42]. Spin can can be taken into account in the local spin density (LSD) approximation [43, 44], *i.e.*

$$\epsilon_{xc}[n(\mathbf{r})] \longrightarrow \epsilon_{xc}[n_\uparrow(\mathbf{r}), n_\downarrow(\mathbf{r})]. \tag{2.14}$$

This is a reasonable first approximation for many systems [45].

Perhaps the most commonly used exchange-correlation approximation is the next rung on the ladder, the generalized gradient approximation (GGA) where also the gradient of the electron density is taken into account [46, 47]

$$E_{xc}^{GGA} = \int n(\mathbf{r})\epsilon_{xc}[\nabla n(\mathbf{r}), n(\mathbf{r}), \mathbf{r}] \, d\mathbf{r}. \tag{2.15}$$

The most popular GGA-functional is the one proposed by Perdew, Burke, and Ernzerhof, namely the PBE functional [48], however there exists a wide range of GGAs [49].

The rung thereafter contains semi-local functionals, often called meta-GGAs [50], which incorporate the kinetic energy of the Kohn-Sham orbitals $\tau(\mathbf{r}) = \sum_{i=1}^{N} \frac{1}{2}|\nabla\psi_i(\mathbf{r})|^2$ or the second derivatives of the electron density $\nabla^2 n(\mathbf{r})$ into the exchange-correlation functional.

To improve the accuracy further, we would need to abandon the local or semi-local picture of the exchange-correlation and go to hybrid functionals, which mix in *exact exchange* in the exchange-correlation functional [49],

$$E_{xc}^{hybrid} = E_{xc}^{GGA} + a \left(E_x^{exact} - E_x^{GGA} \right). \tag{2.16}$$

Exact exchange is used in Hartree-Fock theory and derives from the indiscernible particles principle for fermions. Since the electrons are identical, exchanging particle i and j must give the same result. The energy associated with this is [51]

$$E_x^{exact} = -\frac{1}{2} \sum_{i,j} \int \int \frac{\psi_i^*(\mathbf{r})\psi_j^*(\mathbf{r}')\psi_j(\mathbf{r})\psi_i(\mathbf{r}')}{|\mathbf{r} - \mathbf{r}'|} \, d\mathbf{r} \, d\mathbf{r}', \tag{2.17}$$

which is very similar to the Hartree energy (2.9), but with i and j exchanged. Hybrid functionals are much more computationally demanding than GGAs or meta-GGAs as the exact exchange integration is non-local and in principle stretches over the entire system. The even higher rungs on Jacob's ladder deal more explicitly with the correlation part, *e.g.* the random-phase approximation [52–54].

2.2.1 van der Waals interaction

The lower rungs of the ladder, local and semi-local functionals, clearly miss the van der Waals interaction, as this interaction is non-local and long-range correlation by nature. Perhaps the most pragmatic way of dealing with van der Waals correction is the Grimme formalism [55], where a $1/r^6$ term is parametrized to effectively capture the van der Waals interaction (in analogy to the simple Lennard-Jones pair-potential [56, 57]). Recently, Tkatchenko and Scheffler [58] introduced a parameter-free van der Waals description where the $1/r^6$ coefficients are calculated from the density. A more stringent way to include this nonlocal, long-ranged interaction is with a response integral of the form

$$E_c^{nl} = \frac{1}{2} \int n(\mathbf{r})\phi(\mathbf{r}, \mathbf{r}')n(\mathbf{r}') \, d\mathbf{r} \, d\mathbf{r}', \tag{2.18}$$

as introduced by Lundqvist *et al.* [59], where they put forth appropriate expressions for the kernel $\phi(\mathbf{r}, \mathbf{r}')$. This formalism if often called vdW-DF.

One of the van der Waals functionals used in this thesis is the optB86b-vdW functional [60], which uses Becke-86 exchange [61], LDA correlation, and long-range van der Waals correlation according to the vdW-DF formalism,

$$E_{xc} = E_x^{GGA} + E_c^{LDA} + E_c^{nl}. \tag{2.19}$$

Another semi-local functional that includes the contributions of the response integral in eq. (2.18) is the fitted and trained bayesian error estimation functional (BEEF-vdW) [62].

2.3 Basis set

To solve the Kohn-Sham equations numerically, the orbitals are expanded in a basis set, *i.e.*

$$\psi_i = \sum_j c_{ij}\chi_j, \tag{2.20}$$

where χ_j are the basis functions. Inserting this into the Kohn-Sham equation

$$\sum_j c_{ij}\hat{H}|\chi_j\rangle = \varepsilon_i \sum_j c_{ij}|\chi_j\rangle, \tag{2.21}$$

and multiplying with $\langle\chi_k|$ from the left we obtain the *secular equation*,

$$\sum_j c_{ij}\langle\chi_k|\hat{H}|\chi_j\rangle = \varepsilon_i \sum_j c_{ij}\langle\chi_k|\chi_j\rangle \Leftrightarrow \hat{H}_{kj}C_j = \varepsilon_i S_{kj}C_j, \tag{2.22}$$

or in vector form

$$(\mathbf{H} - \varepsilon_i\mathbf{S})\,\mathbf{C} = \mathbf{0}. \tag{2.23}$$

Here we have the matrix representation of the Kohn-Sham hamiltonian $\mathbf{H}$, the overlap matrix $\mathbf{S}$, the Kohn-Sham eigenvalues ε_i and the basis coefficients $\mathbf{C}$. This matrix problem is what is solved in a DFT software. In the following paragraphs, some different aspects of the choice of basis set will be discussed.

2.3.1 Real-space grid

Perhaps the most straightforward choice is to use a uniform real-space grid, as implemented in the GPAW software [37, 63]. A real-space basis can, however, be tricky since it can depend rather strongly on the position of the grid points. Therefore the energy will not decrease monotonously when the number of grid points is increased. One advantage is that parallelization is comparably easy in real space, which makes it possible to study large systems.

2.3.2 Local basis functions

Another basis set, commonly used, are local functions centred around each atom. There are different types of local basis functions including gaussian-type orbitals, slater-type orbitals, and numerical orbitals [27]. In general local basis function sets can offer reasonable accuracy for a small number of basis functions [64], and are generally computationally cheap. However, it is difficult to know the degree of convergence with respect to the basis set size, since different basis sets can be qualitatively different. Another potential drawback is the so called basis set superposition error, which is a consequence of the non-zero overlap of basis functions around different atoms. In other words the overlap matrix is not just the identity matrix, $S_{kj} = \langle \chi_k | \chi_j \rangle \neq \delta_{kj}$. This means that two or more local basis functions around different atoms can describe the same region in space. This makes it, for instance, difficult but doable to calculate forces. Further, the basis set is often associated with a cut-off radius, where, if outside, the overlap between basis functions is not evaluated. In the DMol^3 software, numerical basis functions are used. They are considered to be of high quality and are supposed minimize basis set superposition effects [65].

2.3.3 Plane-waves

When studying a periodic system, plane waves are a natural choice of basis set, owing to their inherent periodicity. The Vienna Ab-initio Simulation Package (VASP) [66, 67] is a plane-wave basis set code that has been used in this thesis.

In this approach, the Kohn-Sham orbitals are written as a sum over plane-waves:

$$\psi_j = \sum_{\mathbf{k}} c_{j\mathbf{k}} e^{i\mathbf{k}\cdot\mathbf{r}}, \tag{2.24}$$

where the overlap is zero and $S_{ij} = \delta_{ij}$. This can be viewed as Fourier components to the Kohn-Sham orbitals, and by including plane-waves with a higher frequency, more rapidly varying features in the Kohn-Sham orbitals can be described. Therefore, the energy will decrease monotonously with the number of plane-wave basis functions included[3].

In a plane-wave basis set approach, some operations are more readily evaluated in the reciprocal k-space, meaning that Fourier transforms back and forth are involved. This is often not a severe limitation, but becomes computationally expensive for large systems [37].

---

[3]Assuming enough plane-waves initially so the energy is decently described.

2.4   Calculating vibrational frequencies

Vibrations are small movements, deviations from the equilibrium positions of the atoms. For these vibrations, electrons are naturally important, especially if there are very directional bonds, and thereby localized electronic states, between atoms which will result in a restoring force towards the equilibrium configuration. Electronic structure calculations are therefore suitable for calculating vibrational frequencies.

Frequencies for these vibrations are often calculated in a perturbative manner, by expanding the potential around the equilibrium position $\mathbf{r}_0$, and truncating at the second order. In other words writing the potential as [68, p. 520]

$$V\left(\mathbf{r}\right) = V\left(\mathbf{r}_0\right) + \sum_i \left.\frac{\partial V}{\partial r_i}\right|_{\mathbf{r}_0} \Delta r_i + \frac{1}{2}\sum_{i,j} \left.\frac{\partial^2 V}{\partial r_i \partial r_j}\right|_{\mathbf{r}_0} \Delta r_i \Delta r_j + ... \qquad (2.25)$$

where the first term is a constant and will just shift the energy scale and the first order derivative is by definition zero since $\mathbf{r}_0$ is the equilibrium position. The second order derivative is the harmonic term, which can be evaluated through the forces on each atom when displacing each atom,

$$\Delta V\left(\mathbf{r}\right) \simeq \frac{1}{2}\sum_{i,j} \left.\frac{\partial^2 V}{\partial r_i \partial r_j}\right|_{\mathbf{r}_0} \Delta r_i \Delta r_j = -\frac{1}{2}\sum_{i,j} \left.\frac{\partial F_i}{\partial r_j}\right|_{\mathbf{r}_0} \Delta r_i \Delta r_j. \qquad (2.26)$$

By evaluating these force changes, *e.g.* with DFT, the resulting matrix problem can be diagonalized and the eigenvalues will correspond to the harmonic frequencies squared, in analogy to the quantum harmonic oscillator [33]

$$\hat{H}_i = -\frac{1}{2}\frac{\partial^2}{\partial y_i^2} + \frac{1}{2}m\omega_i^2 y_i^2 \qquad (2.27)$$

where y_i are the eigenmodes. By diagonalizing the matrix problem, the eigenenergies can be obtained as

$$E_{i,n} = \hbar\omega_i\left(n + \frac{1}{2}\right), \quad n = 0, 1, 2, ... \qquad (2.28)$$

and the corresponding eigenvector will be the vibrational mode. This estimation of the vibrational frequencies of a system is very useful for interpreting infrared spectroscopy measurements and for calculating vibrational energies and entropies (see chapter 3). By including higher order terms in the expansion of the potential in eq. (2.25), anharmonic effects can be included.

2.5   Finding transition states

The lowest energy barrier between two reaction intermediates, say R and P, is found over a ridge or a saddle point in the energy landscape, having a negative gradient only in one direction, along the *reaction path*. This saddle point, or *transition state*, is necessary to find in order to calculate kinetic reaction barriers. To find reaction barriers and transition
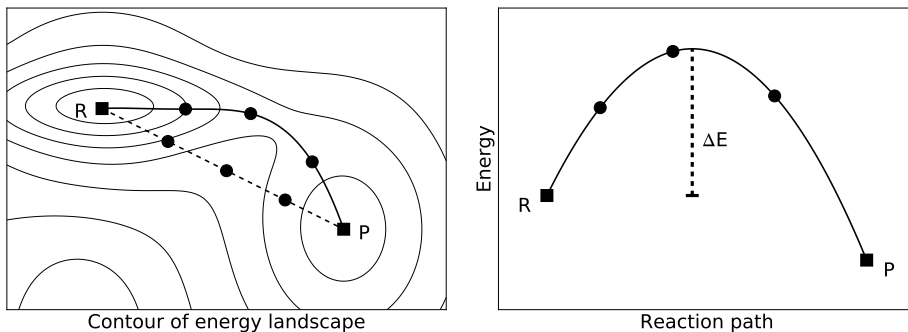
Figure 2.1: Illustration of a nudge elastic band method. To the left, an initial guess (dashed) for the reaction path and then the final path over the saddle point (solid) is found with a series of minmizations perpendicular to the reaction path. To the right, the energy profile along the minimum energy path.

states it is common to use a nudge elastic band (NEB) algorithm, or the improvement climbing image NEB [69–71]. The idea behind the NEB method is to first construct a series of images that connect the reactant and product states, by for example interpolating linearly between the two geometries. By coupling the images with spring forces along the reaction coordinate, and minimizing the forces perpendicular to this direction, the lowest energy path will be found[4]. See figure 2.1 for an illustration. The climbing image NEB algorithm will move the image closest to the saddle point closer to the maximum, by moving it in the opposite direction of the maximum force.

An alternative to the NEB method is the *dimer* method [72, 73], which only uses two images that is moved to the nearest saddle point through a series of translations and rotations. Yet another method for finding transitions states is the Linear Synchronous Transit (LST) [74] where the reaction path is constructed by interpolating between reactant and optimized orthogonally to the reaction path. In the DMol^3 software it is used together with a Quadratic Synchronous Transit (QST) method that uses three structures to interpolate the reaction path.

---

[4]Or to be more precise, the lowest energy path closest to the initial guess will be found.

Chapter 3

Statistical physics and microkinetic modelling

Statistical physics, or statistical mechanics, describes a microscopic way of thinking about thermodynamics. Everything is based on the number of ways in which to arrange a system in *microstates*, and it is a powerful way of connecting energies and electronic structure calculations to macroscopic quantities and behaviours. This chapter is meant to give an overview of this method, and how DFT energies and statistical physics connects to the macroscopic world.

It all starts with identifying an active site, where the reaction takes place, and considering what reactions can happen with different adsorbed molecules and constructing a reaction mechanism, relaxing these adsorbates to obtain energies with *e.g.* DFT, calculating partition functions and rates, solving the kinetic model, and extracting interesting properties like the total rate (turn-over frequency). But let's start from the statistical picture and the probability of observing a certain state.

3.1 The statistical picture

The fundamental assumptions of statistical physics is that all microstates are equally probable in a closed system with constant energy (U), volume (V), and number of particles (N). The probability of finding such a system in a non-degenerate microstate is

$$\mathcal{P} = \frac{1}{W},\tag{3.1}$$

where W is the total number of microstates. For a system degenerate by Ω the probability is

$$\mathcal{P}(\Omega) = \frac{\Omega}{W}.\tag{3.2}$$

This is why all particles in the air do not all gather in one corner of the room, there are just so many more ways of distributing the particles evenly throughout the room [75]. The quantity that governs the physics in this ensemble is the entropy, defined through

$$S = k_{\mathrm{B}} \ln \Omega.\tag{3.3}$$

The most probable configuration is that with the highest entropy, or the largest degeneracy Ω.

In reality, however, it is more likely that the temperature is constant, rather than the energy. This can be taken into account by connecting the system to a large reservoir that can exchange energy with the system, and thereby keep the temperature constant. In

such a system, with constant temperature (T), volume (V), and number of particles (N), the probability of a state is given by the Boltzmann distribution

$$\mathcal{P}(s) = \frac{e^{-E(s)/k_{\mathrm{B}}T}}{\displaystyle\sum_{s} e^{-E(s)/k_{\mathrm{B}}T}} = \frac{e^{-E(s)/k_{\mathrm{B}}T}}{\mathcal{Z}}, \tag{3.4}$$

where $E(s)$ is the energy of the system, k_{B} is Boltzmann's constant, and the sum over states (Zustandssumme in German) $\mathcal{Z}$ is the *canonical partition function*. The physics in this ensemble is governed by the Helmholtz free energy

$$F = -k_{\mathrm{B}}T \ln\left(\mathcal{Z}\right), \tag{3.5}$$

and the most probable state is the state with the lowest free energy.

Often it is easier to keep the pressure constant, rather than the volume, and in such a *Gibb's ensemble* with constant temperature (T), pressure (p), and number of particles (N), the free energy is given by $G = F + pV$. When contemplating relative free energies from a computational perspective, the volume change is often negligible and $\Delta G \approx \Delta F$ [76].

All of this connects to quantum mechanical calculations through the energy. Given a set of energies for different configurations $E(s)$, arrangements of atoms *et cetera*, we can calculate the free energy and thereby determine which configuration is more probable.

3.1.1 Partition functions of adsorbates

Considering an adsorbed molecule on a catalyst's surface, the partition function can be written as a product of the various separable degrees of freedom

$$\mathcal{Z} = Z_{\mathrm{trans}}\, Z_{\mathrm{vib}}\, Z_{\mathrm{rot}}\, Z_{\mathrm{elec}}\, Z_{\mathrm{nucl}}. \tag{3.6}$$

Since we are interested in reactions on surfaces, going from an adsorbed reactant R to a product P, it is unlikely that the sum over the nuclei states will change. We will therefore focus on the others.

The most common expression for the translational partition function is derived from the ideal gas where the particles have kinetic energy $E = \mathbf{p}^2/2m$. In the one-dimensional case the partition function can then be written as an integral[1] over all positions and momenta

$$Z_{\mathrm{trans}}^{\mathrm{1D}} = \frac{1}{h} \int\limits_{0}^{l} \mathrm{d}x \int\limits_{-\infty}^{\infty} e^{-p_x^2/2mk_{\mathrm{B}}T}\, \mathrm{d}p_x = l\frac{(2\pi m k_{\mathrm{B}}T)^{\frac{1}{2}}}{h}. \tag{3.7}$$

In three dimensions the partition function generalizes to

$$Z_{\mathrm{trans}}^{\mathrm{3D}} = V\frac{(2\pi m k_{\mathrm{B}}T)^{\frac{3}{2}}}{h^3} = \frac{V}{\Lambda^3}, \tag{3.8}$$

---

[1]Since phase space can be divided into small cells with side h.

where Λ is the thermal wavelength (the de Broglie wavelength), and is just a convenient way of writing the partition function.[2] The characteristic dimension l or V is the length or volume in which the particle moves. Volume is often less straightforward to use than the pressure of a gas. In many cases it is a good approximation to connect V and the pressure p through the ideal gas law

$$V = \frac{k_B T}{p}. \tag{3.9}$$

Assuming a harmonic potential around the local minima in the potential energy surface, the vibrational energies are those of the quantum harmonic oscillator:

$$E_{i,n} = \hbar \omega_i \left(n + \frac{1}{2} \right), \quad n = 0, 1, 2, ... \tag{3.10}$$

Using these energies in the partition function we obtain

$$Z_{\text{vib}} = \sum_{n=0}^{\infty} e^{-\hbar \omega_i \left(n + \frac{1}{2} \right)/k_B T} = \frac{e^{-\frac{1}{2}\hbar \omega_i / k_B T}}{1 - e^{-\hbar \omega_i / k_B T}}, \tag{3.11}$$

where the nominator is the zero-point energy (the energy for $n = 0$).

Rotations of molecules are essentially treated in the same way. From the energy levels of rotation, assuming a rigid rotor and that the distance between the atoms is fixed[3] the partition function for a polyatomic molecule can be written as [19, p. 92]

$$Z_{\text{rot}} = \frac{1}{\sigma} \left(\frac{8\pi^2 k_B T}{h^2} \right)^{\frac{3}{2}} \sqrt{\pi I_A I_B I_C}, \tag{3.12}$$

where I_A, I_B, and I_C are the moments of inertia along the three principal axes, and σ is the symmetry factor, an orientational degeneracy. For the molecules used in this thesis the symmetry number is $\sigma = 1$ for methanol (no orientational degeneracy), 12 for methane (you can rotate it in many ways and obtain the same structure), and 2 for any diatomic molecule [77, p. 162].

Often we consider adsorbed species to have only vibrational degrees of freedom, while any rotations or translations are well described as in a harmonic potential. If this is not the case, there are ways around it. One different approach is to consider the adsorbates to be a free translator, using a two-dimensional ideal-gas expression for the partition function. If there is a small diffusion barrier between two sites, this can be taken into account with the partition function for a hindered translator. Another rigorous approach is to sample the energy surface along the surface by moving the adsorbates systematically and the partition function can be calculated by integrating over the energy surface. A recent paper by Jørgensen and Grönbeck compares these different approximations for CO oxidation over Pt(111) [78].

---

[2]There is however an assumption that $V/\Lambda^3 \gg 1$ behind all this, *i.e.* that the wavelength of the particle must be much smaller than the length of the container in which it is confined.

[3]It would complicate things considerably if we do not, and it will only result in a small correction.

3.2 Microkinetic modelling - connecting to catalytic reactions

One common way of connecting calculated microscopic quantities, such as energies, structures, and vibrational frequencies to macroscopic quantities, *e.g.* turn-over frequencies, is by constructing a microkinetic model that describes the reaction rates between reactants, intermediates, and products. This tells us something about the time evolution of a system, which steps are important, and lets us extract measurable quantities such as apparent activation energies,turn over frequencies, and kinetic bottlenecks.

3.2.1 Transition state theory

Instead of resolving all energetic states as a function of all the positions and momenta of all particles, the time evolution of a reaction is often modelled as hopping between different local minima, across a saddle point in the free energy landscape. The probability of observing the system in a certain state α must then be written down as a gain-loss relation often called the Master Equation [79]:

$$\frac{\mathrm{d}\mathcal{P}_\alpha}{\mathrm{d}t} = \sum_\beta \left[W_{\beta \to \alpha} \mathcal{P}_\beta - W_{\alpha \to \beta} \mathcal{P}_\alpha \right], \tag{3.13}$$

where $W_{\alpha \to \beta}$ is the transition frequency for jumping from state α to state β, and $\mathcal{P}_\alpha$ is the probability of the system being in state α. A common approximation is to consider an average system, in a mean-field approximation. The probability of being in the state α is then given by the average concentration of α, often denoted θ_α.

Now we only need an expression for the transition frequency. In conventional transition state theory (TST) [80, 81] a reaction is considered to proceed from a reactant R through an activated reaction intermediate $R^\ddagger$, called a transition state (TS), to a product P. The reactant state and the transition state is assumed to obey Boltzmann statistics and recrossing the energy landscape once the transition state has been crossed is not allowed [82]. This can be summarized as

$$R \longleftrightarrow R^\ddagger \longrightarrow P. \tag{3.14}$$

However, relabelling R and P the transition frequency in the other direction can be obtained.

Considering a reaction through a transition state, the frequency at which a chemical reaction happens can be expressed as

$$W_{R \to P} = \nu \frac{\mathcal{P}(R^\ddagger)}{\mathcal{P}(R)} = \nu \frac{\mathcal{Z}^\ddagger}{\mathcal{Z}} = \frac{k_\mathrm{B}T}{h} \frac{\mathcal{Z}^\ddagger}{\mathcal{Z}}. \tag{3.15}$$

The ratio between the sums of available states for R and $R^\ddagger$, given by the partition functions, gives the probability of being in the activated reaction intermediate compared to the reactant. The trial frequency ν is generally considered to be the frequency of the *reaction coordinate*, which is the vibration crossing the saddle point between R and P. In

the classical limit, assuming $h\nu >> k_B T$, it can be proven that the trial frequency equals $k_B T/h$, which at least dimensionally is a frequency. See for example [19, 82] for further details. The reaction coordinate is along one degree of freedom, so $\mathcal{Z}^\ddagger$ has one degree of freedom less.

Separating out the electronic part and expressing the partition function with reference to the local energy minima, the transition rate can be expressed as

$$W_{R \to P} = \frac{k_B T}{h} \frac{\mathcal{Z}'^\ddagger}{\mathcal{Z}'} e^{-\Delta E/k_B T} \equiv k_{\text{TST}}. \tag{3.16}$$

where ΔE is the energy barrier between the transition state and the reactant[4]. This is how the TST rate coefficient is expressed, we "only" need to calculate the partition functions for the transition state $R^\ddagger$ and the different reaction intermediates R and P to get the forward and backward rate constants.

3.3 Putting the pieces together

Now that we have a way of expressing the reaction rates, we can briefly discuss how to put it all together. First of all, we will need a reaction mechanism. This can be simple and linear, $A + B \to AB$ for instance, in which case the gain-loss equation corresponding to the change in concentration of A would be

$$\frac{d\theta_A}{dt} = k_{A+B \to AB} \theta_A \theta_B - k_{AB \to A+B} \theta_{AB}, \tag{3.17}$$

or much more complex with different side reactions and cycles. If A is adsorbed on a surface, θ_A is often called the fractional coverage of A, and is a number between 0 and 1. Notice that the probability of A meeting B and forming AB is proportional to the concentration of A times the concentration of B, $\theta_A \theta_B$, this is the *law of mass action* and within a mean-field approximation. If we have a more complicated reaction mechanism, it is then "just" a matter of keeping track of all reactions and coverages when putting together the loss-gain equations. An example of the time evolution obtained from solving the loss-gain equations numerically is shown in figure 3.1. Here the sequential reaction $A \leftrightarrow B \leftrightarrow C$ is considered, starting from only A species. Here we see that an initial transient behaviour where there is a small coverage of B species eventually turns into a steady state, when the solution is stable with time.

3.3.1 Gas-phase adsorptions

Another aspect we need to be aware of is how to model gas-phase adsorptions, especially non-activated adsorption. We can use transition state theory, but then we need to use expressions for gas-phase systems. This is done by considering the molecule to go from a three-dimensional gas to a two-dimensional gas on the surface, and that there is no barrier $\Delta E = 0$, *i.e.*

$$k_{\text{ads}} = \frac{k_B T}{h} \frac{\mathcal{Z}_{\text{trans}}^{\text{2D}}}{\mathcal{Z}_{\text{trans}}^{\text{3D}}} = \frac{k_B T}{h} \frac{l^3}{\Lambda^3} \frac{\Lambda^2}{l^2} = \frac{\Lambda}{h} p A, \tag{3.18}$$

---

[4]and a positive number.
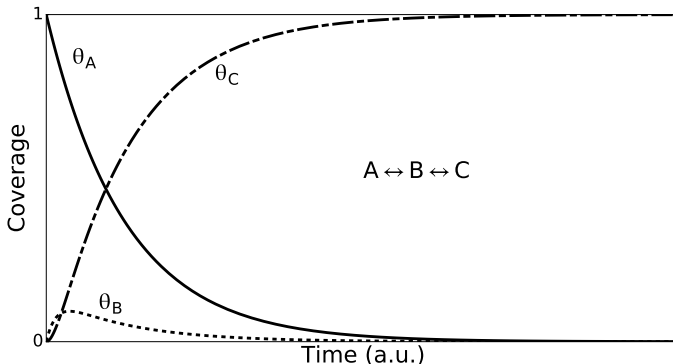
Figure 3.1: Example of the time-dependent solution for a linear $A \leftrightarrow B \leftrightarrow C$ reaction.

where in the last step we have applied the ideal gas law in (3.9), and $l^2 = A$ is the characteristic area in which the adsorbed molecule moves. Here we have assumed that all molecules approaching the surface successfully adsorbs. Generally, an adsorption is not always successful and can depend on the orientation of the molecule as it approaches, where on the surface the molecule hits *et cetera*. This is often introduced in an efficiency coefficient, or *sticking coefficient* [19, 82]. Putting the sticking coefficient to one, as we implicitly did above, gives an upper limit of the rate of adsorption.

The desorption rate, *i.e.* the backward rate, can be defined through the fact that

$$\frac{k_{R \to P}}{k_{P \to R}} = \frac{\mathcal{Z}^\ddagger / \mathcal{Z}_R}{\mathcal{Z}^\ddagger / \mathcal{Z}_P} = \frac{\mathcal{Z}_P}{\mathcal{Z}_R} = e^{\ln \mathcal{Z}_P - \ln \mathcal{Z}_R} = e^{-\Delta G / k_\mathrm{B} T}, \tag{3.19}$$

where ΔG is the free energy difference between the product and initial state. This is also called the *equilibrium constant* K_eq. This means that we can calculate the desorption coefficient as

$$k_\mathrm{des} = k_\mathrm{ads} \frac{\mathcal{Z}_\mathrm{des}}{\mathcal{Z}_\mathrm{ads}} \tag{3.20}$$

From an implementation point of view, the question of how to define the desorption if there is no back-adsorption (consider for example a flow reactor where the products are continuously being removed) can be difficult. Should the desorption event be a function of the pressure dependent adsorption (which does not exist) or not? There is a way around this, by rewriting the partition function for the desorbed state as

$$\mathcal{Z}_\mathrm{des} = Z_\mathrm{surface} \, Z_\mathrm{gas,trans} \, Z_\mathrm{gas,rot} \, Z_\mathrm{gas,vib}, \tag{3.21}$$

where we look at the separate parts for the empty surface and the gas-phase molecule. Plugging this into equation (3.20) and using the known expressions for $Z_\mathrm{gas,trans}$ and k_ads

we get

$$k_{\text{des}} = \frac{\Lambda}{h} \, p \, A \frac{k_{\text{B}}T}{p\Lambda^3} \frac{Z_{\text{surface}} \, Z_{\text{gas,rot}} \, Z_{\text{gas,vib}}}{Z_{\text{ads,vib}}} e^{-\Delta E / k_B T} \tag{3.22}$$

$$= \frac{k_{\text{B}}T}{h} \frac{A}{\Lambda^2} \frac{Z_{\text{surface}} \, Z_{\text{gas,rot}} \, Z_{\text{gas,vib}}}{Z_{\text{ads,vib}}} e^{-\Delta E / k_B T}, \tag{3.23}$$

where ΔE is the energy difference between the adsorbed and desorbed systems. This is, from an implementation point of view, much more useful since it is pressure independent.

3.4 The mean-field approximation

An observant reader might have noticed that the mean-field approximation was used in eq. (3.17) without much justification. The mean-field approximation assumes that all adsorbed species are randomly distributed on the catalytic surface and that there is no interaction between the adsorbed species [19]. If there is lateral interaction (especially attractive interaction) between adsorbates, the rate of A reacting with B is not just $\theta_A \theta_B$, as assumed in section 3.3. The alternative to using a mean-field model is to perform a fully stochastic Monte Carlo simulation [79].

For catalysts with isolated sites (like zeolites which will be introduced in the next chapter), the distance to the neighbouring site is large and the interaction weak, and the sites can be treated independently. For theses systems, the mean-field approximation should work and the mean-field coverages θ_i correspond to the fractional number of sites of each intermediate i. As a first approximation, for the molybdenum sulfide clusters we have used a mean-field kinetic model, even though there are lateral interactions. Some lateral interaction is implicitly included in the energy calculations.

3.5 Degree of rate control

Given a net rate of a reaction, *i.e.* how many times per second a product is produced, we can perform a sensitivity analysis to attempt to unravel the behaviour of the reaction. One way to do this is to perform a *degree of rate control* analysis, as proposed by Campbell *et al.* [83, 84]. In this scheme, the rate coefficients k_i (or equivalently the barriers) are changed and the response of the total rate r is examined. In a normalized way, this corresponds to

$$X_{\text{RC},i} = \frac{k_i}{r} \left(\frac{\partial r}{\partial k_i} \right)_{k_{j \neq i}, K_i}, \tag{3.24}$$

where i is each step in the reaction mechanism. K_i indicates that the equilibrium constant is conserved and the thermodynamics of the reaction is not altered.

Chapter 4

Partial methane oxidation

> ''
>   Ironically, the direct conversion of methane to derivatives, e.g., methanol,
> is thermodynamically feasible, but kinetically difficult.

> – Pei Tang *et al.* [85]

Methane is not the most energetically favourable configuration of carbon and hydrogen. With access to oxygen, we all remember from high school chemistry that the most favourable configuration is CO_2 and water. So, how can methane be only partially oxidized into something more useful than CO_2? It would require a catalyst that helps to control the reactions and steer the selectivity towards, for instance, methanol. This chapter will discuss some of the catalysts we know can do this and how the work reported in this thesis aims to understand and potentially improve the selectivity of methane oxidation.

4.1   What is needed for partial methane oxidation?

Partial oxidation of methane with oxygen from the air would be a dream reaction [86]

$$CH_4 + \frac{1}{2}O_2 \rightarrow CH_3OH. \tag{4.1}$$

In the same spirit, the ultimate goal is also to do this reaction at *ambient conditions*, *i.e.* atmospheric pressure and room temperature. Present methanol synthesis is far from fulfilling this. Currently, industrial conversion of methane into methanol and other chemicals is done in a two-step process, where methane (or to be more correct natural gas) is transformed into synthesis gas, or syngas (CO and H_2) [14], which can then be used to create a wide spectrum of hydrocarbons or alcohols [87, 88]. This is done in very large centralized plants, which is not in line with the very dispersed methane reserves in the world. A direct conversion of methane to methanol in one step would be a considerably more efficient route. However, this reaction is associated with intriguing challenges and has not yet been industrialized [13, 88].

In some way, everything begins with the methane activation, breaking the first C-H bond. This is tricky because methane is a very stable molecule, has the strongest C-H bond of all hydrocarbons [85], a high free energy barrier at normal conditions[1], and is highly symmetric with no obvious attacking point. Things are further complicated by the fact that methanol is not the thermodynamically most favourable product of methane and oxygen, as is obvious from figure 4.1.

---

[1]Low enthalpic barriers are not uncommon on many catalyst, but the entropic barrier at elevated temperatures is significant.
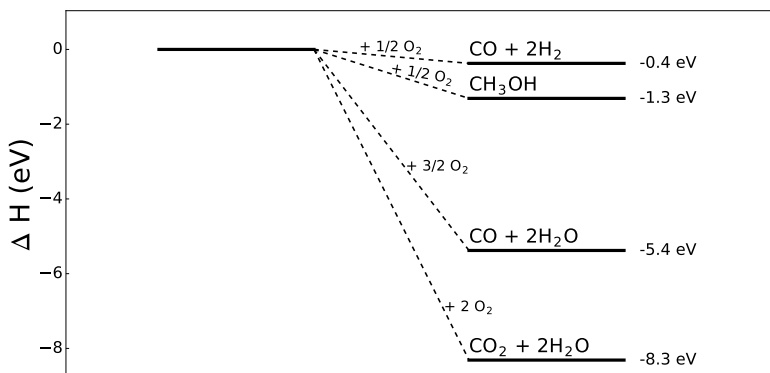
Figure 4.1: Diagram of different reaction enthalpies starting from methane and adding oxygen [85, 88, 89].

Another issue is the activation of the stable oxygen molecule. This is certainly also a requirement, and not an easy one. To eliminate this particular problem, it could be a nice idea to use another oxygen source. In some cases, laughing gas N_2O is used. From a sustainability point of view it would, however, be better to use O_2.

The reaction seems impossible based on the previously mentioned problems. There are, never the less, systems in nature that actually can convert methane to methanol. The main example being the natural enzymes methane monooxygenases (MMO) [90–92]. The exact nature of the active sites in MMO is still a topic of discussion. There seems to be some consensus that in the different MMOs, di-metallic centres of iron or copper are involved. A less controversial feature of the MMOs is that they have a porous structure. This is believed to be important for selectivity. With a restricted pore size, large molecules and reactants can not enter and get to the active site, and large products cannot be created. Although MMO can convert methane to methanol there are some shortcomings, *e.g.* a very low production rate. For an industrial and efficient implementation this is a serious shortcoming. It can also be difficult to separate out the products with this homogeneous catalytic reaction, since these enzymes exist in a solution. With a heterogeneous catalytic system that could convert methane to methanol, separating out the liquid methanol, as compared to other gases, would be much easier and therefore more desirable.

Steering the selectivity towards methanol is difficult. One reason we have not yet discussed is that once you have broken the first C-H bond, breaking all the others is easier and you strip off all hydrogen atoms, ending up with CO or CO_2. On an ordinary extended surface or nanoparticle with large facets, this is possible since you have many neighbouring sites where the other hydrogen atoms can end up. What you have in the enzymes, is isolated sites with a long distance to the next active site. Single-site catalysis in this way seem to be a requirement for partial oxidation of methane.
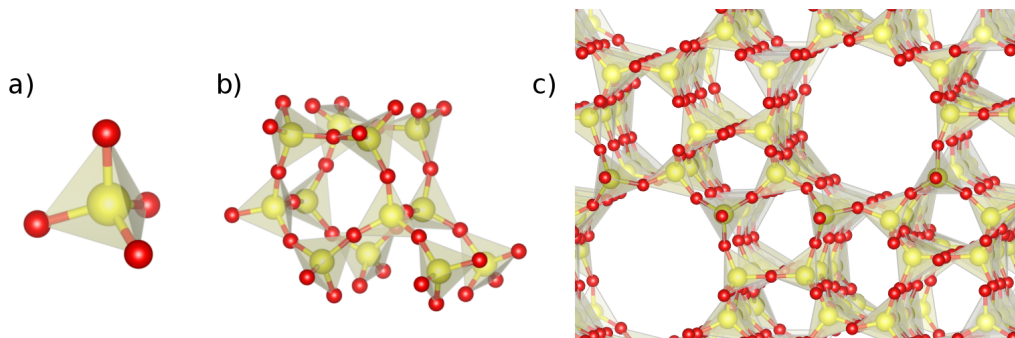
Figure 4.2: Zeolites are built from tetrahedras, T-sites in (a) into secondary building units, SBU in (b), which can then be combined into the full periodic structure in (c). Here the MFI framework is used as an example.

4.2 Zeolites

Zeolites are a class of materials that are readily used in industrial catalysis [93]. They are sometimes viewed as inorganic analogues to the methane monooxygenase (MMO) enzyme and similarly have pores and metal ion sites. Zeolites ion-exchanged with certain ions, *e.g.* Cu, Ni, Co, and Fe, have been shown to be able to convert methane to methanol at ambient conditions [94–99].

Zeolites are formed by corner-sharing SiO_4 and AlO_4 tetrahedrons, often called T-sites (see figure 4.2). They are generally thermodynamically meta-stable and template molecules are used in the synthesis. Around these template molecules the silicon oxide can be grown in various ways, depending on what template you use, creating pores and cages of different sizes. Some examples are Mordenite, Chabasite, and MFI [93, 100]. ZSM-5 is an example of the latter and is especially interesting when it comes to partial methane oxidation.

By replacing Si^{4+} with Al^{3+}, a net charge is created which is compensated by a counter ion. When synthesized, the counter ion can be Na^+, a proton, H^+, or ammonia [101]. In a later stage, these can be ion-exchanged with different cations to something more interesting, like Cu, Fe, Co, or Ni. Cu-exchanged ZSM-5 is one of the most studied systems and the system studied in this thesis.

How these metal ions are arranged depends to some extent on the aluminium distribution. Given a Si:Al ratio, there exists a distribution of Al T-sites [102]. Two Al atoms can not be neighbouring T-sites and share the same oxygen, this is called Löwenstein's rule [103, 104]. Other than this rule, we know that the distribution of Al and the number of Al pairs can be controlled to some degree depending on the synthesis method [105, 106]. The number of Al pairs can be important, since depending on the number of Al T-sites per cation, the oxidation state of the metal ion can vary. The common oxidation states for Cu are 1+ and 2+ [107], indicating that one Cu cation can in principle compensate the charge of one or two Al T-sites [108].

4.2.1 Cu-ZSM-5

One of the most studied systems for heterogeneous direct conversion of methane to methanol is copper-exchanged ZSM-5 [94, 99, 101, 109–117]. The first successful experimental observation of methane-to-methanol conversion at ambient conditions, atmospheric pressure and a temperature of 448 K, required O_2-activation at much higher temperature (723 K) and the methanol had to be extracted in a third stage with a water/acetonitrile mixture [94]. This makes the process unattractive for any industrial application. One reason for the need of an extraction solvent, could be that water reduces the methanol desorption barrier, as suggested by recent calculations [118]. A continuous catalytic cycle has recently been demonstrated [21, 22], but an efficient methane-to-methanol conversion has still not been obtained. By understanding how the Cu-ZSM-5 system works, the hope is that we will be able to design an even better catalyst. However, first we need to understand the three steps during the reaction: the oxygen activation, the partial oxidation of methane, and the methanol extraction. Moreover, we need to know which active sites are involved in the reaction.

4.2.2 The mystery of the active site

There have been many attempts to try and determine the active sites in metal ion-exchanged zeolites [21, 94, 96, 101, 109–111, 113, 115, 118–134].

For Cu-exchanged zeolites, a $[Cu-O-Cu]^{2+}$ motif has been suggested as a possible candidate. This motif was experimentally identified with a characteristic spectroscopic signature in the UV-vis region around $22\,700\,cm^{-1}$. The appearance of this signature for zeolites with different Cu:Al ratio correlated with the methanol production [94]. This signature was later assigned to a bent $[Cu-O-Cu]^{2+}$ structure [114].

Since the $[Cu-O-Cu]^{2+}$ motif was identified, it has been extensively characterized, both experimentally and theoretically [114, 117, 135]. The $[Cu-O-Cu]^{2+}$ motif is a good candidate for active site, however the absolute need for this motif for methane-to-methanol conversion is not conclusive. For instance, Narsimhan *et al.* [21] were recently able to
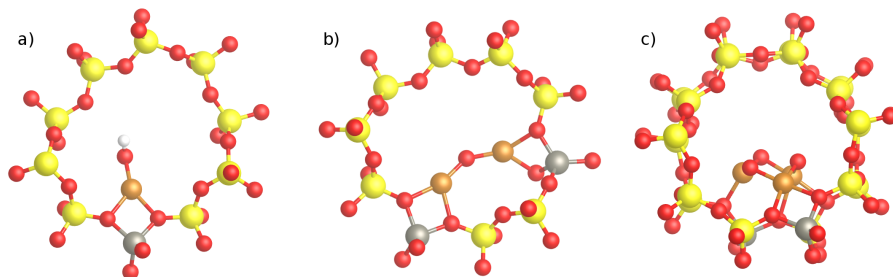
Figure 4.3: Three candidate for active sites: a) $[CuOH]^+$ b) $[Cu-O-Cu]^{2+}$ c) $[Cu_3O_3]^{2+}$. Colour code: silicon (yellow), oxygen (red), aluminium (grey), copper (brown), hydrogen (white). The structure in c) is adapted from [109].

24

(a) Model size convergence

(b) Energy landscapes
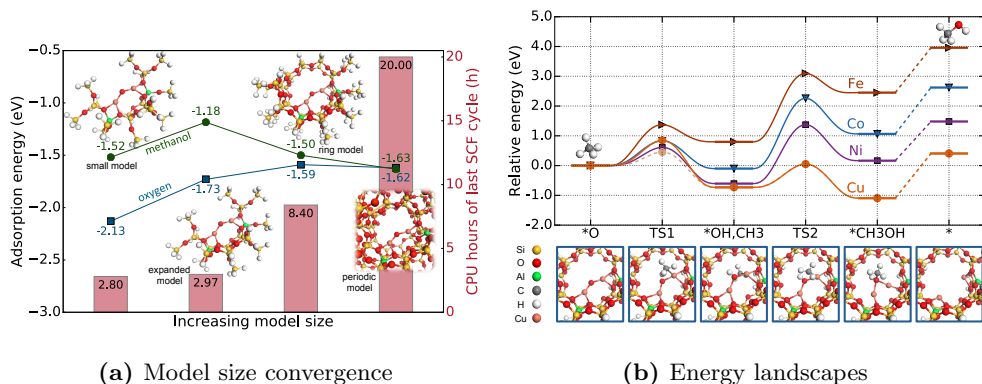
Figure 4.4: (a) Adsorption energies of oxygen and methanol for different model sizes for the $[Cu-O-Cu]^{2+}$ motif, and on the right vertical axis computational cost for one self-consistent cycle. (b) Calculated energy landscapes for methane-to-methanol conversion over ZSM-5 for Cu, Ni, Co, and Fe dimer sites from **Paper I**.

experimentally demonstrate a continuous catalytic methane-to-methanol cycle in Cu-ZSM-5 without the appearance of the UV-vis signature around $22\,700\,cm^{-1}$. Also, in recent theoretical studies [109, 136], trinuclear Cu-clusters were suggested as possible active sites in Cu-Mordenite and Cu-ZSM-5, while Kulkarni *et al.*[137] suggest a Cu monomer site in addition to the $[Cu-O-Cu]^{2+}$ and Cu_3O_3 motifs. However, the $[Cu-O-Cu]^{2+}$ motif is still a viable, but perhaps not the only, candidate for an active site.

4.3 Metal dimer sites in ZSM-5

In **Paper I**, we study the $[Cu-O-Cu]^{2+}$ motif, for Cu and other transition metals by means of DFT and micro-kinetic modelling. In a study by Tsai *et al.* [135], the different possible configurations of a $[Cu-O-Cu]^{2+}$ motif in the ZSM-5 zeolite was investigated. They found that there is a clear energetically favourable configuration at the crossing between the straight and sinusoidal channels. Using this, we constructed a cluster model of the active site, *i.e.* a piece from the periodic structure around the active site. The first question we addressed was how much of the structure we need to include in the cluster model to accurately describe the true periodic system. With different sizes of the cluster model we compared the adsorption energies of oxygen and methanol on the dimer motif, compared to the periodic structure (see figure 4.4a). The results show that including the whole ring structure of the pore around the active site seems to be important. It is also clear that using the *ring model* is a good compromise between accuracy in energy and computational cost.
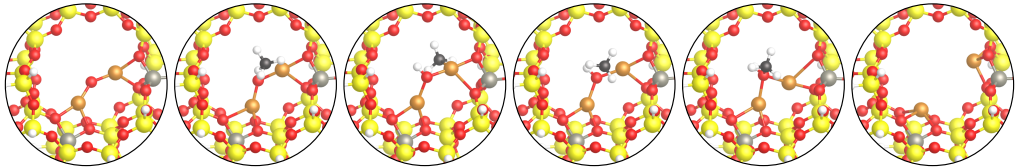
Figure 4.5: Reaction mechanism for methane-to-methanol conversion starting from the [Cu-O-Cu]$^{2+}$ motif to the left (*O), and then subsequently TS1, (*OH,CH3), TS2, (*CH3OH), and to the right the empty site (*).

Once we decided for the ring model, we considered a simple and direct reaction mechanism, namely

$$^*O + CH_4 \underset{k_1}{\rightleftarrows} \,^*OH, CH_3 \tag{4.2}$$

$$^*OH, CH_3 \underset{k_2}{\rightleftarrows} \,^*CH_3OH \tag{4.3}$$

$$^*CH_3OH \underset{k_3}{\rightleftarrows} \,^* + CH_3OH \tag{4.4}$$

with a first step of dissociative adsorption of methane with the formation of adsorbed -OH and -CH$_3$ groups. The second step is the subsequent recombination of these groups into adsorbed methanol (*CH$_3$OH), and a third step with methanol desorption, see figure 4.5. We study two cases, a steady state case which includes methanol back-adsorption, and one transient model which does not, *i.e.* setting $k_3^- = 0$. This would correspond to the case when methanol is continuously and rapidly extracted from the reaction. Here we have assumed a mean-field distribution of adsorbed species and used ideal-gas expressions for the free molecules. Another restriction is that we do not consider the oxygen activation, since it is not fully understood. One possibility is a formation of a peroxo intermediate (Cu-O-O-Cu) [116] followed by subsequent removal of the first and then the second oxygen atom.

The energies of intermediates and transition states for the [Cu-O-Cu]$^{2+}$ motif was calculated for Cu, Ni, Co, and Fe (see figure 4.6). As can be seen in the figure, we considered two methane dissociation barriers for Cu: the geometrically shortest reaction path through what resembles a surface-stabilized transition state with a -CH$_3$-group bound to one of the copper ions, and another path through a CH$_3$ radical-like transition state. Recently Latimer *et al.* [138, 139] have described these two different methane activation pathways, finding different scaling relations and arguably different physics for different classes of catalysts. Using the climbing image NEB method, we did not find the radical barrier. When using the alternative LSTQST method, as applied in the DMol^3 software, we did find a radical-like TS for Cu. Although this barrier is 0.39 eV lower than the surface-stabilized, the sensitivity analysis (see section 4.3.1) reveals that it is only for Cu the first barrier is rate-determining, while the Ni, Co, and Fe systems remain unaffected by changes in the methane dissociation barrier. It also shows that the surface-stabilized or the radical barrier does not make a difference for the trend in elements.
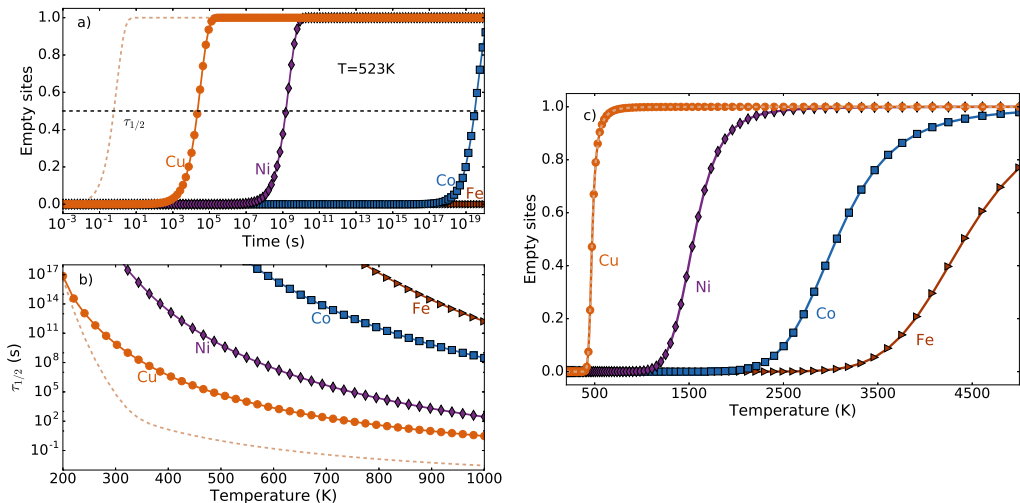
Figure 4.6: a) Coverage of empty sites, or methanol produced, for the Cu, Ni, Co and Fe dimer sites as a function of time at 523 K. b) The reaction time $\tau_{1/2}$ as a function of temperature. c) Steady-state coverages of empty sites for the Cu, Ni, Co and Fe dimer sites as a function of temperature. The dashed lines for Cu are for the radical-like methane dissociation barrier.

The micro-kinetic results for experimental conditions of 1 mbar and 523 K are shown in figure 4.6. This shows a clear trend in catalytic performance (here measured with the half-time $\tau_{1/2}$ when half of the methane has been converted) between the different dimer sites. The time scale is reasonable for Cu, while unrealistically long for Ni, Co and Fe. To put this into perspective, the Big-bang theory puts the age of the universe at 13.8 billion years or $4.4 \cdot 10^{17}$ s [140, 141]. The steady state kinetics with a methanol pressure of 10^{-6} bar is shown in figure 4.6. Here we see that the $[Cu-O-Cu]^{2+}$ site converts methane to methanol around 500 K, while Ni, Co, and Fe require unrealistically high temperatures. One measure of this is that the ZSM-5 framework actually breaks around 1400 K [142]. Since there exists experimental evidence for methane-to-methanol conversion for Ni-, Co- and Fe-ZSM-5 zeolites [95–97], there is obviously something wrong with our assumptions. This can mean either that for Ni, Co and Fe, the proposed reaction mechanism is not correct, or that this dimer motif is not a relevant active site for these zeolites.

27
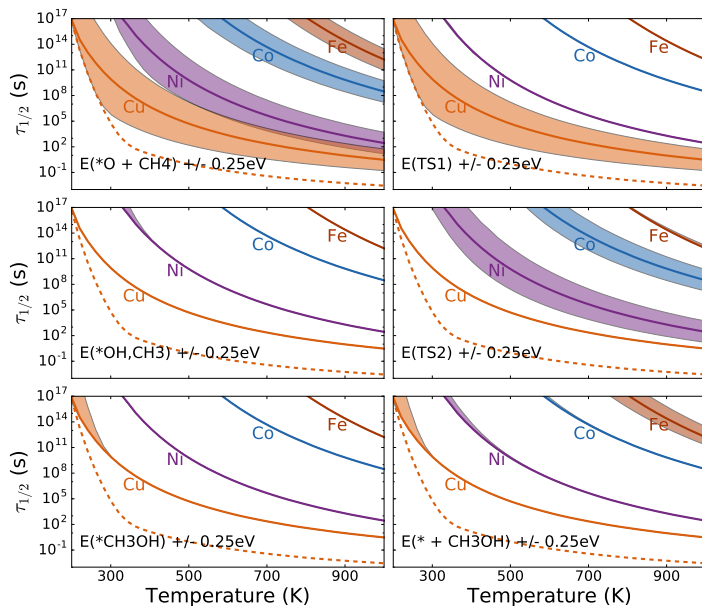
Figure 4.7: Change in $\tau_{1/2}$ when changing the energy of each intermediate by $\pm 0.25\,\text{eV}$. From **Paper I**.

4.3.1 Sensitivity analysis

To evaluate which step is important, we changed the energy of each step by $\pm 0.25\,\text{eV}$ for Cu, Ni, Co, and Fe, and evaluated the changes in the kinetic behaviour (see figure 4.1). This demonstrates that the conclusion, that Cu is the best, followed by Ni, Co, and Fe, is robust and would not change by using a different energy description, *e.g.* including van der Waals interactions. An energy change of $\pm 0.25\,\text{eV}$ is of the same order of magnitude as the shift in adsorption energies in zeolites when including van der Waals interaction [143]. The sensitivity analysis also shows that the methane dissociation barrier (TS1) is important only for Cu, while TS2 is important for Ni and Co, and the desorbed methanol state is important for Fe. The energy of the oxygenated site *O + CH4 is important for all considered metals. This analysis confirms that the trend in elements, Cu followed by Ni, Co, and then Fe, is robust and that the surface-stabilized or radical-like methane dissociation barrier does not change that conclusion.

4.4 Infrared spectroscopy study

In **Paper II** infrared spectroscopy experiments together with frequency calculations were used to investigate methanol interaction with the zeolite. Comparing the experimental spectra at different temperatures, for Cu-exchanged ZSM-5 and bare ZSM-5, it is clear that the Cu species are responsible for most of the interaction with methanol. One
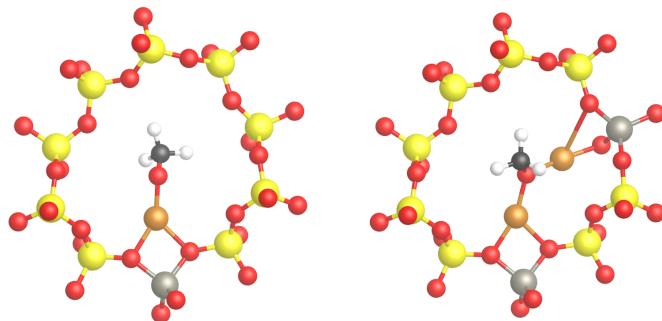
Figure 4.8: Methoxy bound to a copper monomer (left) and a dimer (right).

main conclusion from the experiments is that CO and formate, OCHO, peaks are only observed for the Cu-exchanged zeolite, indicating that the Cu-species are responsible for the further oxidation of methanol to CO and formate. The calculations presented here confirm, together with other experimental literature that these peaks are indeed CO and OCHO on a copper monomer site, see table 4.1. Frequencies were calculated for adsorbates on the $[Cu-O-Cu]^{2+}$ motif, a Cu monomer, a Brønsted acid site (Al + H+). One interesting feature of the calculated frequencies is the shift in one of the C-H stretching modes for methoxy (OCH_3) adsorbed on the Cu monomer site, see figure 4.8. Compared to methoxy on the dimer motif, one of the three C-H stretching modes has a low frequency at $2693\,\mathrm{cm}^{-1}$, compared to the others around 2900-$3000\,\mathrm{cm}^{-1}$. The largest discrepancy between the calculated wavenumbers and the experimental literature is for the proton on the Brønsted acid site, $3103\,\mathrm{cm}^{-1}$ compared to $3620\,\mathrm{cm}^{-1}$ in literature [126, 144–146].

4.5 Molybdenum sulfide clusters

Another approach that we have started in **Paper III** is to use sulfur as oxidant, H_2S to be more precise, and a Mo_6S_8 cluster as catalyst. This also has a single-site character, especially if the system is promoted with one Ni or K atom. Here, the reaction mechanism has been to consider a mean-field model for a double-site denoted [A*,B*], symbolizing an -S-Mo- site with A adsorbed to the sulfur and B on the molybdenum. We consider H_2S and CH_4 dissociation, H_2 formation, and the direct recombination of a [*,SH*] and

Table 4.1: Calculated wavenumbers (cm^{-1})

Adsorbate	Cu monomer	Cu dimer	Al + H$^+$	Bare
CH$_3$OH	2941.5, 3024.1, 3148.4, 3761.3	2970.5, 3079.8, 3095.3, 3413.1	2909.3, 2991.3, 3056.0, 3421.2	– –
OCH$_3$	2692.9, 2930.2, 2983.8	2903.1, 2986.5, 3015.8	2968.2, 3063.6, 3078.8	–
OH	3631.6	3580.1	3102.8	3618.1
CO	2124.0	–	–	–
HOC=O	1614.4, 2924.2	–	–	–
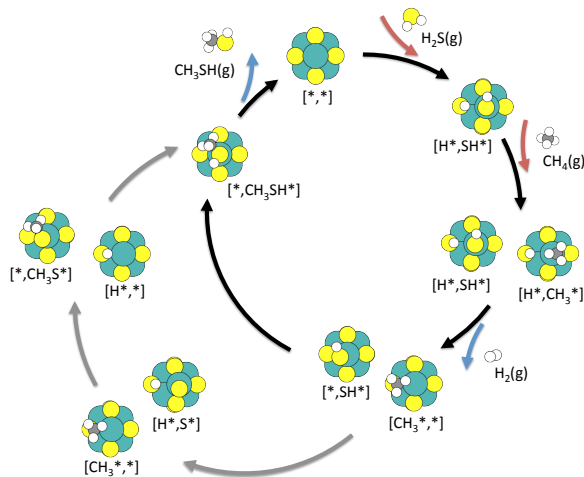
Figure 4.9: Reaction mechanism for CH_4 oxidation with H_2S to CH_3SH and H_2 on Mo_6S_8 clusters from **Paper III**. A direct recombination of a CH_3^* and and SH^* species (black arrows) and a longer stepwise recombination (grey arrows).

$[CH_3^*,^*]$ species to CH_3SH, as illustrated in figure 4.9.

With the mentioned notation, this would correspond to

$$H_2S(g) + [^*,^*] \underset{k_1}{\rightleftarrows} [^*, H_2S^*], \tag{4.5}$$

$$[^*, H_2S^*] \underset{k_2}{\rightleftarrows} [H^*, SH^*], \tag{4.6}$$

$$CH_4(g) + [^*,^*] \underset{k_3}{\rightleftarrows} [^*, CH_4^*], \tag{4.7}$$

$$[^*, CH_4^*] \underset{k_4}{\rightleftarrows} [H^*, CH_3^*], \tag{4.8}$$

$$[H^*, CH_3^*] + [^*,^*] + [H^*, SH^*] \underset{k_5}{\rightleftarrows} [CH_3^*,^*] + [^*, H_2^*] + [^*, SH^*], \tag{4.9}$$

$$[^*, H_2^*] \underset{k_6}{\rightleftarrows} [^*,^*] + H_2(g), \tag{4.10}$$

$$[CH_3^*,^*] + [^*, SH^*] \underset{k_7}{\rightleftarrows} 2[^*,^*] + CH_3SH(g), \tag{4.11}$$
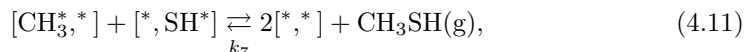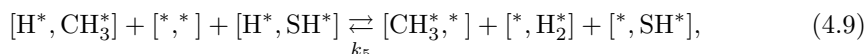
for the bare Mo_6S_8 and the K-promoted cluster, although the site preference, *i.e.* the absolute association of A to the S atom and B to the Mo atom may change. For the Ni-promoted cluster, differences in the energetics motivate the use of a slightly different reaction mechanism (see figure 4.10), *e.g.* it is more energetically favourable to have two H* on the same cluster, meaning that the fourth and fifth step in the mechanism will be

30
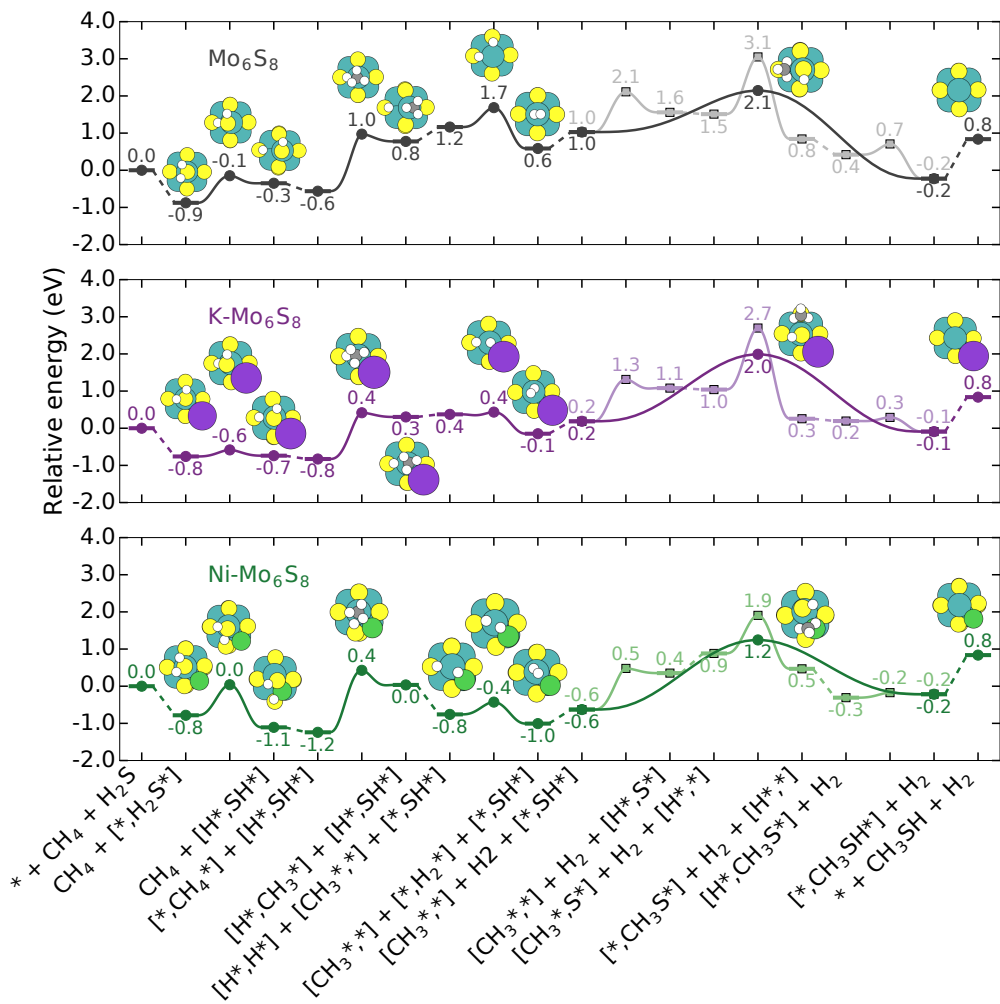
Figure 4.10: Energy landscapes for the Mo_6S_8 clusters with the longer stepwise pathway in a lighter shade, from **Paper III**.

(a) Turn-over frequencies

(b) Degree of rate control
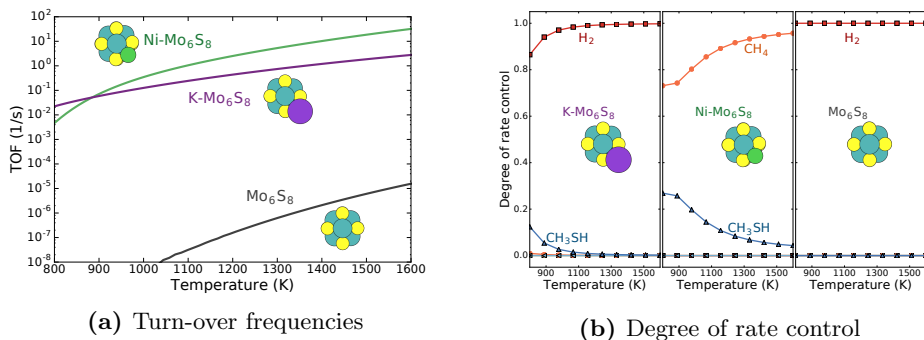
Figure 4.11: Turn-over frequencies for all clusters in (a) and degree of rate control in (b) as a function of temperature for the K- and Ni-promoted Mo_6S_8 clusters.

changed to:

$$[CH_4^*, ^*] + [^*, ^*] + [H^*, SH^*] \underset{k_4}{\rightleftarrows} [CH_3^*,] + [H^*, H^*] + [^*, SH^*], \tag{4.12}$$

$$[H^*, H^*] \underset{k_5}{\rightleftarrows} [^*, H_2^*]. \tag{4.13}$$
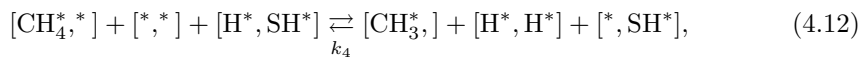
These lateral effects are not considered explicitly other than in the energy calculations. Energies for a longer, stepwise reaction path through [CH_3^*,S^*] and [H^*,CH_3S^*] to yield [*,CH_3SH^*] were also evaluated. This reaction path was however not considered for the kinetic modelling since the barriers were higher (the more lightly shaded curves in figure 4.10).

The turnover frequency (see figure 4.11a) clearly shows that the promoted Mo_6S_8 clusters are far superior to the bare cluster. Which promotor is better changes with temperature, this behaviour is investigated further with a degree of rate control analysis (see figure 4.11b). The rate-determining step for K-Mo_6S_8 at high temperature is the hydrogen formation, while for Ni-Mo_6S_8 the methane dissociation is controlling. At lower temperatures ($<900\,\mathrm{K}$) the Ni-promoted cluster becomes limited by the CH_3SH desorption, an effect that also is reflected in the TOF in figure 4.11a, where Ni enters a non-linear regime with prohibiting coverage effects.

Chapter 5

Conclusions and outlook

The aim of this thesis has been to investigate partial oxidation of methane, primarily into methanol, using Cu-exchanged ZSM-5, and to understand the different aspects of direct methane-to-methanol conversion. This has been done by combining electronic structure calculations and microkinetic modelling, and comparing with experiments via vibrational analysis.

By comparing adsorption energies for different model sizes, we showed that it is important to include enough of the pore structure to accurately describe adsorbates on the $[Cu-O-Cu]^{2+}$ site in ZSM-5. The study of the metal dimer motif in **Paper I** also shows that the $[Cu-O-Cu]^{2+}$ is a relevant candidate for active site only in Cu-ZSM-5. Furthermore, we showed that the methane dissociation barrier is only important for the Cu motif, and even though the two different barriers, one surface-stabilized and one radical-like, evaluated for Cu differ with almost $0.4\,eV$, the conclusion that the dimer motif is reasonable for Cu, but not realistic for Ni, Co, or Fe, did not change. It does, however, raise the question for future work, which barrier is correct, especially since a climbing NEB algorithm does not find the radical-like barrier.

The comparison between experimental and calculated infrared frequencies in **Paper II** confirms that Cu species in Cu-ZSM-5 are responsible for the further oxidation of methanol to carbon monoxide and formate. Calculated frequencies for methoxy on a copper monomer give one C-H stretching mode close to a broad peak seen in experiments. This needs to be investigated further. The calculated O-H stretch for the Brønsted acid site differs significantly from the experimental assignment. If this could depend on the site we model should also be considered in the future.

Paper III demonstrates that partial oxidation of methane should also be possible on Mo_6S_8 clusters, but that promoting the clusters is necessary, here we tried Ni or K and found that both are more active. We plan to continue this project further by expanding the reaction mechanism to include other products and start looking at selectivity. It would also be interesting to see if methanol can be a product on these clusters with water as an oxidant.

Acknowledgements

I would also like to thank:

My main supervisor Anders Hellman, for simply being the best supervisor there is. A constant source of inspiration and optimism, especially time optimism (if there's such a word in Anglo-Saxon). But with your support and encouragement it always works out for the best.

My examiner and assistant supervisor Henrik Grönbeck, for all the help, support, and for all discussions.

Per-Anders Carlsson, for all support and discussions.

"My" experimentalist Xueting Wang. Your the best, Ting! Talking with you, asking you about experiments and anything else is always a joy.

My officemates: Mikael, Maxime and Matthias, you are the best room mates on M, Pooya the greatest officemate on P I've ever had, Adriana the nicest on A. Thank you all for putting up with me, my questions and discussions.

Everyone at Chemical Physics for creating a nice atmosphere. In particular Unni, Mikkel, Alvaro, Lin, Lucy, Michael, Baochang, Junais, Fredrik, Oskar, Matthias, Mikael, and Maxime. The rest of the Theory Council. Thank you for keeping the council the best council there is at Chemical Physics.

Igor for letting me ask tricky questions and for asking questions back.

Daniel for being a great friend and for all the good times spent planning and improving teaching. Consider yourself acknowledged.

All KCK members, co-authors, friends, and anyone else I forgot to mention. Thank you!

Last but not least, my family. Without you and your support, this would simply not have happened.

<div style="text-align: right;">Adam Arvidsson, Göteborg, May 2017</div>

Bibliography

[1] J. J. Berzelius. *Årsberättelsen om framsteg i fysik och kemi.* p. 245. Stockholm: Royal Swedish Academy of Sciences, 1835.

[2] G. Ertl. *Gerhard Ertl - Nobel Lecture: Reactions at Surfaces: From Atoms to Complexity.* 2007. URL: `http://www.nobelprize.org/nobel_prizes/chemistry/laureates/2007/ertl-lecture.html` (visited on 04/03/2017).

[3] L. J. Pettersson. *KTH — Jöns Jacob Berzelius - the Man Who Invented Catalysis?* `https://www.kth.se/en/che/archive/arkiv/berzelius-1.184145`. 2013. (Visited on 03/30/2017).

[4] P. Collins. The Pivotal Role of Platinum in the Discovery of Catalysis. *Platinum Metals Review* **30**.3 (1986), 141–146.

[5] J. Wisniak. The History of Catalysis. From the Beginning to Nobel Prizes. *Educación química* **21** (2010), 60–69.

[6] H. Davy. Some New Experiments and Observations on the Combustion of Gaseous Mixtures, with an Account of a Method of Preserving a Continued Light in Mixtures of Inflammable Gases and Air without Flame. *Philosophical Transactions of the Royal Society of London* **107** (1817), 77–85.

[7] *Composition of Natural Gas.* `http://naturalgas.org/overview/background/`. 2013. (Visited on 09/30/2016).

[8] *Statistical Review of World Energy — Energy Economics — BP Global.* `http://www.bp.com/en/global/corporate/energy-economics/statistical-review-of-world-energy.html`. (Visited on 09/30/2016).

[9] C. D. Elvidge et al. Methods for Global Survey of Natural Gas Flaring from Visible Infrared Imaging Radiometer Suite Data. *Energies* **9**.1 (2016), 14. DOI: `10.3390/en9010014`.

[10] J. Lelieveld and P. J. Crutzen. Indirect Chemical Effects of Methane on Climate Warming. *Nature* **355**.6358 (1992), 339.

[11] S. Pacala and R. Socolow. Stabilization Wedges: Solving the Climate Problem for the Next 50 Years with Current Technologies. *Science* **305**.5686 (2004), 968–972. DOI: `10.1126/science.1100103`.

[12] A. Caballero and P. J. Pérez. Methane as Raw Material in Synthetic Chemistry: The Final Frontier. *Chemical Society Reviews* **42**.23 (2013), 8809–8820. DOI: `10.1039/C3CS60120J`.

[13] A. I. Olivos-Suarez et al. Strategies for the Direct Catalytic Valorization of Methane Using Heterogeneous Catalysis: Challenges and Opportunities. *ACS Catalysis* **6**.5 (2016), 2965–2981. DOI: `10.1021/acscatal.6b00428`.

[14] J. R. Rostrup-Nielsen. Production of Synthesis Gas. *Catalysis Today* **18**.4 (1993), 305–324. DOI: `10.1016/0920-5861(93)80059-A`.

[15] *Wikimedia Commons Figure: Catalysis Scheme.* 2017. URL: `https://commons.wikimedia.org/wiki/File:CatalysisScheme.png`.

[16] *Wikimedia Commons Figure: Volcano plot.* 2017. URL: `https://commons.wikimedia.org/wiki/File:Volcano_plot.png`.

[17] V. Smil. Detonator of the Population Explosion. *Nature* **400**.6743 (1999), 415–415.

[18]   A. Hellman et al. "Ammonia Synthesis: State of the Bellwether Reaction". *Comprehensive Inorganic Chemistry II*. Elsevier, 2013, pp. 459–474. DOI: 10.1016/B978-0-08-097774-4.00725-7.

[19]   I. Chorkendorff and J. W. Niemantsverdriet. *Concepts of Modern Catalysis and Kinetics*. John Wiley & Sons, 2006.

[20]   A. F. Cronstedt. Om En Obekant Bärg Art, Som Kallas Zeoliter. *Kongl. Svenska Vetenskaps Academiens Handlingar Stockholm* **17** (1756), 120.

[21]   K. Narsimhan et al. Catalytic Oxidation of Methane into Methanol over Copper-Exchanged Zeolites with Oxygen at Low Temperature. *ACS Central Science* **2**.6 (2016), 424–429. DOI: 10.1021/acscentsci.6b00139.

[22]   B. Ipek and R. F. Lobo. Catalytic Conversion of Methane to Methanol on Cu-SSZ-13 Using N2O as Oxidant. *Chemical Communications* **52**.91 (2016), 13401–13404. DOI: 10.1039/C6CC07893A.

[23]   H. S. Taylor. A Theory of the Catalytic Surface. *Proceedings of the Royal Society of London A: Mathematical, Physical and Engineering Sciences* **108**.745 (1925), 105–111. DOI: 10.1098/rspa.1925.0061.

[24]   R. P. Feynman and R. Leighton. *Surely You're Joking, Mr. Feynman!* W.W. Norton (USA), 1985.

[25]   E. Schrödinger. Quantisierung Als Eigenwertproblem. *Annalen der Physik* **385**.13 (1926), 437–490. DOI: 10.1002/andp.19263851302.

[26]   R. M. Martin. *Electronic Structure: Basic Theory and Practical Methods*. Cambridge: Cambridge Univ. Press, 2004.

[27]   J. Thijssen. *Computational Physics*. Cambridge University Press, 2007.

[28]   M. Born and R. Oppenheimer. Zur Quantentheorie Der Molekeln. *Annalen der Physik* **389**.20 (1927), 457–484. DOI: 10.1002/andp.19273892002.

[29]   W. Kohn. *Walter Kohn - Nobel Lecture: Electronic Structure of Matter - Wave Functions and Density Functionals*. 1999. URL: http://www.nobelprize.org/nobel_prizes/chemistry/laureates/1998/kohn-lecture.html (visited on 05/06/2017).

[30]   L. H. Thomas. The Calculation of Atomic Fields. *Mathematical Proceedings of the Cambridge Philosophical Society* **23**.05 (1927), 542. DOI: 10.1017/S0305004100011683.

[31]   E. Fermi. Statistical Method to Determine Some Properties of Atoms. *Rend. Accad. Naz. Lincei* **6** (1927), 602–607.

[32]   P. Hohenberg and W. Kohn. Inhomogeneous Electron Gas. *Physical Review* **136**.3B (1964), B864–B871. DOI: 10.1103/PhysRev.136.B864.

[33]   J. J. Sakurai and J. Napolitano. *Modern Quantum Mechanics*. 2. ed. Reading, Mass.: Addison-Wesley, 2011.

[34]   W. Kohn and L. J. Sham. Self-Consistent Equations Including Exchange and Correlation Effects. *Physical Review* **140**.4A (1965), A1133–A1138. DOI: 10.1103/PhysRev.140.A1133.

[35]   D. Vanderbilt. Soft Self-Consistent Pseudopotentials in a Generalized Eigenvalue Formalism. *Physical Review B* **41**.11 (1990), 7892–7895. DOI: 10.1103/PhysRevB.41.7892.

[36]   P. E. Blöchl. Projector Augmented-Wave Method. *Physical Review B* **50**.24 (1994), 17953–17979. DOI: 10.1103/PhysRevB.50.17953.

[37] J. Enkovaara et al. Electronic Structure Calculations with GPAW: A Real-Space Implementation of the Projector Augmented-Wave Method. *Journal of Physics: Condensed Matter* **22**.25 (2010), 253202. DOI: 10.1088/0953-8984/22/25/253202.

[38] G. Kresse and D. Joubert. From Ultrasoft Pseudopotentials to the Projector Augmented-Wave Method. *Physical Review B* **59**.3 (1999), 1758–1775. DOI: 10.1103/PhysRevB.59.1758.

[39] R. P. Feynman. Forces in Molecules. *Physical Review* **56**.4 (1939), 340–343. DOI: 10.1103/PhysRev.56.340.

[40] J. D. Head and M. C. Zerner. A Broyden—Fletcher—Goldfarb—Shanno Optimization Procedure for Molecular Geometries. *Chemical Physics Letters* **122**.3 (1985), 264–270. DOI: 10.1016/0009-2614(85)80574-1.

[41] J. P. Perdew and K. Schmidt. "Jacob's Ladder of Density Functional Approximations for the Exchange-Correlation Energy". Vol. 577. AIP Publishing, 2001, pp. 1–20. DOI: 10.1063/1.1390175.

[42] D. M. Ceperley and B. J. Alder. Ground State of the Electron Gas by a Stochastic Method. *Physical Review Letters* **45**.7 (1980), 566–569. DOI: 10.1103/PhysRevLett.45.566.

[43] O. Gunnarsson, B. I. Lundqvist, and S. Lundqvist. Screening in a Spin-Polarized Electron Liquid. *Solid State Communications* **11**.1 (1972), 149–153. DOI: 10.1016/0038-1098(72)91150-7.

[44] O. Gunnarsson and B. I. Lundqvist. Exchange and Correlation in Atoms, Molecules, and Solids by the Spin-Density-Functional Formalism. *Physical Review B* **13**.10 (1976), 4274–4298. DOI: 10.1103/PhysRevB.13.4274.

[45] A. D. Becke. Perspective: Fifty Years of Density-Functional Theory in Chemical Physics. *The Journal of Chemical Physics* **140**.18 (2014), 18A301. DOI: 10.1063/1.4869598.

[46] D. C. Langreth and M. J. Mehl. Beyond the Local-Density Approximation in Calculations of Ground-State Electronic Properties. *Physical Review B* **28**.4 (1983), 1809–1834. DOI: 10.1103/PhysRevB.28.1809. (Visited on 05/08/2017).

[47] A. D. Becke. Density Functional Calculations of Molecular Bond Energies. *The Journal of Chemical Physics* **84**.8 (1986), 4524–4529. DOI: 10.1063/1.450025.

[48] J. P. Perdew, K. Burke, and M. Ernzerhof. Generalized Gradient Approximation Made Simple. *Physical Review Letters* **77**.18 (1996), 3865–3868. DOI: 10.1103/PhysRevLett.77.3865.

[49] S. Kurth, J. P. Perdew, and P. Blaha. Molecular and Solid-State Tests of Density Functional Approximations: LSD, GGAs, and Meta-GGAs. *International Journal of Quantum Chemistry* **75**.4-5 (1999), 889–909.

[50] J. P. Perdew et al. Accurate Density Functional with Correct Formal Properties: A Step Beyond the Generalized Gradient Approximation. *Physical Review Letters* **82**.12 (1999), 2544–2547. DOI: 10.1103/PhysRevLett.82.2544.

[51] A. D. Becke. A New Mixing of Hartree–Fock and Local Density-functional Theories. *The Journal of Chemical Physics* **98**.2 (1993), 1372–1377. DOI: 10.1063/1.464304.

[52] D. Bohm and D. Pines. A Collective Description of Electron Interactions: III. Coulomb Interactions in a Degenerate Electron Gas. *Physical Review* **92**.3 (1953), 609–625. DOI: 10.1103/PhysRev.92.609.

[53] D. C. Langreth and J. P. Perdew. Exchange-Correlation Energy of a Metallic Surface: Wave-Vector Analysis. *Physical Review B* **15**.6 (1977), 2884–2901. DOI: 10.1103/PhysRevB.15.2884.

[54] X. Ren et al. Random-Phase Approximation and Its Applications in Computational Chemistry and Materials Science. *Journal of Materials Science* **47**.21 (2012), 7447–7471. DOI: 10.1007/s10853-012-6570-4.

[55] S. Grimme. Semiempirical GGA-Type Density Functional Constructed with a Long-Range Dispersion Correction. *Journal of Computational Chemistry* **27**.15 (2006), 1787–1799. DOI: 10.1002/jcc.20495.

[56] J. E. Jones. On the Determination of Molecular Fields. II. From the Equation of State of a Gas. *Proceedings of the Royal Society of London A: Mathematical, Physical and Engineering Sciences* **106**.738 (1924), 463–477. DOI: 10.1098/rspa.1924.0082.

[57] J. E. Lennard-Jones. Cohesion. *Proceedings of the Physical Society* **43**.5 (1931), 461. DOI: 10.1088/0959-5309/43/5/301. (Visited on 04/19/2017).

[58] A. Tkatchenko and M. Scheffler. Accurate Molecular Van Der Waals Interactions from Ground-State Electron Density and Free-Atom Reference Data. *Physical Review Letters* **102**.7 (2009), 073005. DOI: 10.1103/PhysRevLett.102.073005.

[59] M. Dion et al. Van Der Waals Density Functional for General Geometries. *Physical Review Letters* **92**.24 (2004), 246401. DOI: 10.1103/PhysRevLett.92.246401.

[60] J. Klimeš, D. R. Bowler, and A. Michaelides. Van Der Waals Density Functionals Applied to Solids. *Physical Review B* **83**.19 (2011), 195131. DOI: 10.1103/PhysRevB.83.195131.

[61] A. D. Becke. On the Large-gradient Behavior of the Density Functional Exchange Energy. *The Journal of Chemical Physics* **85**.12 (1986), 7184–7187. DOI: 10.1063/1.451353. (Visited on 04/19/2017).

[62] J. Wellendorff et al. Density Functionals for Surface Science: Exchange-Correlation Model Development with Bayesian Error Estimation. *Physical Review B* **85**.23 (2012), 235149. DOI: 10.1103/PhysRevB.85.235149.

[63] J. J. Mortensen, L. B. Hansen, and K. W. Jacobsen. Real-Space Grid Implementation of the Projector Augmented Wave Method. *Physical Review B* **71**.3 (2005), 035109. DOI: 10.1103/PhysRevB.71.035109.

[64] H. Grönbeck. First Principles Studies of Metal-Oxide Surfaces. *Topics in Catalysis* **28**.1-4 (2004), 59–69. DOI: 10.1023/B:TOCA.0000024334.52677.67.

[65] B. Delley. An All-electron Numerical Method for Solving the Local Density Functional for Polyatomic Molecules. *The Journal of Chemical Physics* **92**.1 (1990), 508–517. DOI: 10.1063/1.458452.

[66] G. Kresse and J. Furthmüller. Efficiency of Ab-Initio Total Energy Calculations for Metals and Semiconductors Using a Plane-Wave Basis Set. *Computational Materials Science* **6**.1 (1996), 15–50. DOI: 10.1016/0927-0256(96)00008-0.

[67] G. Kresse and J. Furthmüller. Efficient Iterative Schemes for Ab Initio Total-Energy Calculations Using a Plane-Wave Basis Set. *Physical Review B* **54**.16 (1996), 11169–11186. DOI: 10.1103/PhysRevB.54.11169.

[68] D. A. McQuarrie and J. D. Simon. Physical Chemistry: A Molecular Approach. *University Science Book* (1997).

[69]   G. Henkelman, B. P. Uberuaga, and H. Jónsson. A Climbing Image Nudged Elastic Band Method for Finding Saddle Points and Minimum Energy Paths. *The Journal of Chemical Physics* **113**.22 (2000), 9901–9904. DOI: `10.1063/1.1329672`.

[70]   G. Henkelman and H. Jónsson. Improved Tangent Estimate in the Nudged Elastic Band Method for Finding Minimum Energy Paths and Saddle Points. *The Journal of Chemical Physics* **113**.22 (2000), 9978–9985. DOI: `10.1063/1.1323224`.

[71]   D. Sheppard, R. Terrell, and G. Henkelman. Optimization Methods for Finding Minimum Energy Paths. *The Journal of Chemical Physics* **128**.13 (2008), 134106. DOI: `10.1063/1.2841941`.

[72]   G. Henkelman and H. Jónsson. A Dimer Method for Finding Saddle Points on High Dimensional Potential Surfaces Using Only First Derivatives. *The Journal of Chemical Physics* **111**.15 (1999), 7010–7022. DOI: `10.1063/1.480097`.

[73]   A. Heyden, A. T. Bell, and F. J. Keil. Efficient Methods for Finding Transition States in Chemical Reactions: Comparison of Improved Dimer Method and Partitioned Rational Function Optimization Method. *The Journal of Chemical Physics* **123**.22 (2005), 224101. DOI: `10.1063/1.2104507`.

[74]   T. A. Halgren and W. N. Lipscomb. The Synchronous-Transit Method for Determining Reaction Pathways and Locating Molecular Transition States. *Chemical Physics Letters* **49**.2 (1977), 225–232. DOI: `10.1016/0009-2614(77)80574-5`.

[75]   D. V. Schroeder. *An Introduction to Thermal Physics*. International Edition. San Francisco: Addison Wesley Longman, 2000.

[76]   K. Reuter and M. Scheffler. Composition, structure, and stability of $RuO_2(110)$ as a function of oxygen pressure. *Phys. Rev. B* **65**.3 (2001). DOI: `10.1103/PhysRevB.65.035406`. URL: `https://link.aps.org/doi/10.1103/PhysRevB.65.035406`.

[77]   D. A. McQuarrie and J. D. Simon. *Molecular thermodynamics*. University Science Books Sausalito, CA, 1999.

[78]   M. Jørgensen and H. Grönbeck. Adsorbate Entropies with Complete Potential Energy Sampling in Microkinetic Modeling. *The Journal of Physical Chemistry C* (2017). DOI: `10.1021/acs.jpcc.6b11487`.

[79]   A. P. J. Jansen. *An Introduction to Kinetic Monte Carlo Simulations of Surface Reactions*. Springer-Verlag Berlin Heidelberg, 2012.

[80]   H. Eyring. The Activated Complex in Chemical Reactions. *The Journal of Chemical Physics* **3**.2 (1935), 107–115. DOI: `10.1063/1.1749604`.

[81]   M. G. Evans and M. Polanyi. Some Applications of the Transition State Method to the Calculation of Reaction Velocities, Especially in Solution. *Transactions of the Faraday Society* **31** (1935), 875–894.

[82]   G. Mills, H. Jónsson, and G. K. Schenter. Reversible Work Transition State Theory: Application to Dissociative Adsorption of Hydrogen. *Surface Science* **324**.2–3 (1995), 305–337. DOI: `10.1016/0039-6028(94)00731-4`.

[83]   C. T. Campbell. Future Directions and Industrial Perspectives Micro- and Macro-Kinetics: Their Relationship in Heterogeneous Catalysis. *Topics in Catalysis* **1**.3-4 (1994), 353–366. DOI: `10.1007/BF01492288`.

[84]   C. Stegelmann, A. Andreasen, and C. T. Campbell. Degree of Rate Control: How Much the Energies of Intermediates and Transition States Control Rates.

Journal of the American Chemical Society **131**.23 (2009), 8077–8082. DOI: 10.1021/ja9000097.

[85] P. Tang et al. Methane Activation: The Past and Future. *Energy & Environmental Science* **7**.8 (2014), 2580–2591. DOI: 10.1039/C4EE00604F.

[86] R. Horn and R. Schlögl. Methane Activation by Heterogeneous Catalysis. *Catalysis Letters* **145**.1 (2015), 23–39. DOI: 10.1007/s10562-014-1417-z.

[87] A. P. E. York, T. Xiao, and M. L. H. Green. Brief Overview of the Partial Oxidation of Methane to Synthesis Gas. *Topics in Catalysis* **22**.3-4 (2003), 345–358. DOI: 10.1023/A:1023552709642.

[88] A. Holmen. Direct Conversion of Methane to Fuels and Chemicals. *Catalysis Today* **142**.1–2 (2009), 2–8. DOI: 10.1016/j.cattod.2009.01.004.

[89] K. Tabata et al. Activation of Methane by Oxygen and Nitrogen Oxides. *Catalysis Reviews* **44**.1 (2002), 1–58. DOI: 10.1081/CR-120001458.

[90] A. C. Rosenzweig et al. Crystal Structure of a Bacterial Non-Haem Iron Hydroxylase That Catalyses the Biological Oxidation of Methane. *Nature* **366**.6455 (1993), 537–543. DOI: 10.1038/366537a0.

[91] R. Balasubramanian et al. Oxidation of Methane by a Biological Dicopper Centre. *Nature* **465**.7294 (2010), 115–119. DOI: 10.1038/nature08992.

[92] A. E. Shilov and A. A. Shteinman. Methane Hydroxylation: A Biomimetic Approach. *Russian Chemical Reviews* **81**.4 (2012), 291. DOI: 10.1070/RC2012v081n04ABEH004271.

[93] M. Beller, A. Renken, and R. A. van Santen. *Catalysis*. Wiley-VCH, Weinheim, 2012.

[94] M. H. Groothaert et al. Selective Oxidation of Methane by the Bis(μ-Oxo)Dicopper Core Stabilized on ZSM-5 and Mordenite Zeolites. *Journal of the American Chemical Society* **127**.5 (2005), 1394–1395. DOI: 10.1021/ja047158u.

[95] J. Shan et al. Conversion of Methane to Methanol with a Bent Mono(μ-Oxo)Dinickel Anchored on the Internal Surfaces of Micropores. *Langmuir* **30**.28 (2014), 8558–8569. DOI: 10.1021/la501184b.

[96] N. V. Beznis, B. M. Weckhuysen, and J. H. Bitter. Partial Oxidation of Methane Over Co-ZSM-5: Tuning the Oxygenate Selectivity by Altering the Preparation Route. *Catalysis Letters* **136**.1-2 (2010), 52–56. DOI: 10.1007/s10562-009-0206-6.

[97] E. V. Starokon et al. Room-Temperature Oxidation of Methane by α-Oxygen and Extraction of Products from the FeZSM-5 Surface. *The Journal of Physical Chemistry C* **115**.5 (2011), 2155–2161. DOI: 10.1021/jp109906j.

[98] S. E. Bozbag et al. Methane to Methanol over Copper Mordenite: Yield Improvement through Multiple Cycles and Different Synthesis Techniques. *Catalysis Science & Technology* **6**.13 (2016), 5011–5022. DOI: 10.1039/C6CY00041J.

[99] M. J. Wulfers et al. Conversion of Methane to Methanol on Copper-Containing Small-Pore Zeolites and Zeotypes. *Chemical Communications* **51**.21 (2015), 4447–4450. DOI: 10.1039/C4CC09645B.

[100] J. J. Pluth, J. V. Smith, and W. J. Mortier. Positions of Cations and Molecules in Zeolites with the Chabazite Framework. IV Hydrated and Dehydrated Cu2+-Exchanged Chabazite. *Materials Research Bulletin* **12**.10 (1977), 1001–1007. DOI: 10.1016/0025-5408(77)90025-3.

[101] N. V. Beznis, B. M. Weckhuysen, and J. H. Bitter. Cu-ZSM-5 Zeolites for the Formation of Methanol from Methane and Oxygen: Probing the Active Sites and Spectator Species. *Catalysis Letters* **138**.1-2 (2010), 14–22. DOI: 10.1007/s10562-010-0380-6.

[102] B. R. Goodman et al. Statistical Analysis of Al Distributions and Metal Ion Pairing Probabilities in Zeolites. *Catalysis Letters* **68**.1-2 (2000), 85–93. DOI: 10.1023/A:1019066916541.

[103] W. Loewenstein. The Distribution of Aluminum in the Tetrahedra of Silicates and Aluminates. *American Mineralogist* **39**.1-2 (1954), 92–96.

[104] R. G. Bell, R. A. Jackson, and C. R. A. Catlow. Löwenstein's Rule in Zeolite A: A Computational Study. *Zeolites* **12**.7 (1992), 870–871.

[105] O. H. Han, C.-S. Kim, and S. B. Hong. Direct Evidence for the Nonrandom Nature of Al Substitution in Zeolite ZSM-5: An Investigation by 27Al MAS and MQ MAS NMR. *Angewandte Chemie* **114**.3 (2002), 487–490. DOI: 10.1002/1521-3757(20020201)114:3<487::AID-ANGE487>3.0.CO;2-Z.

[106] V. Gábová, J. Dědeček, and J. Čejka. Control of Al Distribution in ZSM-5 by Conditions of Zeolite Synthesis. *Chemical Communications* 10 (2003), 1196–1197. DOI: 10.1039/B301634J.

[107] G. T. Palomino et al. Oxidation States of Copper Ions in ZSM-5 Zeolites. A Multitechnique Investigation. *The Journal of Physical Chemistry B* **104**.17 (2000), 4064–4073. DOI: 10.1021/jp993893u.

[108] F. Göltl, P. Sautet, and I. Hermans. The Impact of Finite Temperature on the Coordination of Cu Cations in the Zeolite SSZ-13. *Catalysis Today*. Advances in Automobile Emissions Control Catalysis **267** (2016), 41–46. DOI: 10.1016/j.cattod.2015.10.028.

[109] G. Li et al. Stability and Reactivity of Copper Oxo-Clusters in ZSM-5 Zeolite for Selective Methane Oxidation to Methanol. *Journal of Catalysis* **338** (2016), 305–312. DOI: 10.1016/j.jcat.2016.03.014.

[110] P. J. Smeets, M. H. Groothaert, and R. A. Schoonheydt. Cu Based Zeolites: A UV–vis Study of the Active Site in the Selective Methane Oxidation at Low Temperatures. *Catalysis Today* **110**.3–4 (2005), 303–309. DOI: 10.1016/j.cattod.2005.09.028.

[111] P. J. Smeets et al. Oxygen Precursor to the Reactive Intermediate in Methanol Synthesis by Cu-ZSM-5. *Journal of the American Chemical Society* **132**.42 (2010), 14736–14738. DOI: 10.1021/ja106283u.

[112] P. Tomkins et al. Isothermal Cyclic Conversion of Methane into Methanol over Copper-Exchanged Zeolite at Low Temperature. *Angewandte Chemie* **128**.18 (2016), 5557–5561. DOI: 10.1002/ange.201511065.

[113] P. Vanelderen et al. Cu-ZSM-5: A Biomimetic Inorganic Model for Methane Oxidation. *Journal of Catalysis*. Molecular Approach to Heterogeneous Catalysis. **284**.2 (2011), 157–164. DOI: 10.1016/j.jcat.2011.10.009.

[114] J. S. Woertink et al. A [Cu2O]2+ Core in Cu-ZSM-5, the Active Site in the Oxidation of Methane to Methanol. *Proceedings of the National Academy of Sciences* **106**.45 (2009), 18908–18913. DOI: 10.1073/pnas.0910461106.

[115]   M. H. Mahyuddin et al. Direct Conversion of Methane to Methanol by Metal-Exchanged ZSM-5 Zeolite (Metal = Fe, Co, Ni, Cu). *ACS Catalysis* (2016), 8321–8331. DOI: `10.1021/acscatal.6b01721`.

[116]   T. Yumura et al. Roles of Water Molecules in Modulating the Reactivity of Dioxygen-Bound Cu-ZSM-5 toward Methane: A Theoretical Prediction. *ACS Catalysis* (2016), 2487–2495. DOI: `10.1021/acscatal.5b02477`.

[117]   P. Haack et al. Access to a CuII–O–CuII Motif: Spectroscopic Properties, Solution Structure, and Reactivity. *Journal of the American Chemical Society* **135**.43 (2013), 16148–16160. DOI: `10.1021/ja406721a`.

[118]   Z.-J. Zhao et al. Theoretical Insights into the Selective Oxidation of Methane to Methanol in Copper-Exchanged Mordenite. *ACS Catalysis* (2016), 3760–3766. DOI: `10.1021/acscatal.6b00440`.

[119]   M. H. Groothaert et al. Identification of Cu(II) Coordination Structures in Cu-ZSM-5, Based on a DFT/Ab Initio Assignment of the EPR Spectra. *Physical Chemistry Chemical Physics* **5**.10 (2003), 2135–2144. DOI: `10.1039/B301120H`.

[120]   B. F. Mentzen and G. Bergeret. Crystallographic Determination of the Positions of the Copper Cations in Zeolite MFI. *The Journal of Physical Chemistry C* **111**.34 (2007), 12512–12516. DOI: `10.1021/jp075452d`.

[121]   T. Yumura et al. Effects of ZSM-5 Zeolite Confinement on Reaction Intermediates during Dioxygen Activation by Enclosed Dicopper Cations. *Inorganic Chemistry* **48**.2 (2009), 508–517. DOI: `10.1021/ic8010184`.

[122]   N. V. Beznis et al. Oxidation of Methane to Methanol and Formaldehyde over Co–ZSM-5 Molecular Sieves: Tuning the Reactivity and Selectivity by Alkaline and Acid Treatments of the Zeolite ZSM-5 Agglomerates. *Microporous and Mesoporous Materials* **138**.1–3 (2011), 176–183. DOI: `10.1016/j.micromeso.2010.09.009`.

[123]   E. V. Starokon et al. Mechanisms of Iron Activation on Fe-Containing Zeolites and the Charge of α-Oxygen. *Topics in Catalysis* **23**.1-4 (2003), 137–143. DOI: `10.1023/A:1024832606400`.

[124]   C. Hammond et al. Direct Catalytic Conversion of Methane to Methanol in an Aqueous Medium by Using Copper-Promoted Fe-ZSM-5. *Angewandte Chemie International Edition* **51**.21 (2012), 5129–5133. DOI: `10.1002/anie.201108706`.

[125]   D. Nachtigallová et al. Coordination and Siting of Cu+ Ions in ZSM-5: A Combined Quantum Mechanics/Interatomic Potential Function Study. *Physical Chemistry Chemical Physics* **1**.8 (1999), 2019–2026. DOI: `10.1039/A900214F`.

[126]   A. B. Ene et al. Adsorption of Oxygen on Copper in Cu/HZSM5 Zeolites. *Physical Chemistry Chemical Physics* **12**.24 (2010), 6520–6531. DOI: `10.1039/C000750A`.

[127]   G. Li et al. Stability of Extraframework Iron-Containing Complexes in ZSM-5 Zeolite. *The Journal of Physical Chemistry C* **117**.1 (2013), 413–426. DOI: `10.1021/jp310374k`.

[128]   P. Vanelderen et al. Spectroscopic Definition of the Copper Active Sites in Mordenite: Selective Methane Oxidation. *Journal of the American Chemical Society* **137**.19 (2015), 6383–6392. DOI: `10.1021/jacs.5b02817`.

[129]   E. M. C. Alayon et al. Reaction Conditions of Methane-to-Methanol Conversion Affect the Structure of Active Copper Sites. *ACS Catalysis* **4**.1 (2014), 16–22. DOI: `10.1021/cs400713c`.

[130] E. M. C. Alayon et al. Bis(μ-Oxo) versus Mono(μ-Oxo)Dicopper Cores in a Zeolite for Converting Methane to Methanol: An in Situ XAS and DFT Investigation. *Physical Chemistry Chemical Physics* **17**.12 (2015), 7681–7693. DOI: 10.1039/C4CP03226H.

[131] F. Göltl et al. Computationally Exploring Confinement Effects in the Methane-to-Methanol Conversion Over Iron-Oxo Centers in Zeolites. *ACS Catalysis* (2016), 8404–8409. DOI: 10.1021/acscatal.6b02640.

[132] M. He et al. Theoretical Study on Methane Oxidation Catalyzed by Fe/ZSM-5: The Significant Role of Water on Binuclear Iron Active Sites. *The Journal of Physical Chemistry C* (2016). DOI: 10.1021/acs.jpcc.6b09548.

[133] C. Paolucci et al. Catalysis in a Cage: Condition-Dependent Speciation and Dynamics of Exchanged Cu Cations in SSZ-13 Zeolites. *Journal of the American Chemical Society* **138**.18 (2016), 6028–6048. DOI: 10.1021/jacs.6b02651.

[134] L. Vilella and F. Studt. The Stability of Copper Oxo Species in Zeolite Frameworks. *European Journal of Inorganic Chemistry* **2016**.10 (2016), 1514–1520. DOI: 10.1002/ejic.201501270.

[135] M.-L. Tsai et al. [Cu2O]2+ Active Site Formation in Cu–ZSM-5: Geometric and Electronic Structure Requirements for N2O Activation. *Journal of the American Chemical Society* **136**.9 (2014), 3522–3529. DOI: 10.1021/ja4113808.

[136] S. Grundner et al. Single-Site Trinuclear Copper Oxygen Clusters in Mordenite for Selective Conversion of Methane to Methanol. *Nature Communications* **6** (2015), 7546. DOI: 10.1038/ncomms8546.

[137] A. R. Kulkarni et al. Monocopper Active Site for Partial Methane Oxidation in Cu-Exchanged 8MR Zeolites. *ACS Catalysis* (2016), 6531–6536. DOI: 10.1021/acscatal.6b01895.

[138] A. A. Latimer et al. Understanding Trends in C-H Bond Activation in Heterogeneous Catalysis. *Nature Materials* **16**.2 (2017), 225–229. DOI: 10.1038/nmat4760.

[139] A. A. Latimer et al. Mechanistic Insights into Heterogeneous Methane Activation. *Physical Chemistry Chemical Physics* **19**.5 (2017), 3575–3581. DOI: 10.1039/C6CP08003K.

[140] *Big-Bang Model — Cosmology*. https://global.britannica.com/topic/big-bang-model. (Visited on 04/29/2017).

[141] C. L. Bennett et al. Nine-Year Wilkinson Microwave Anisotropy Probe (WMAP) Observations: Final Maps and Results. *The Astrophysical Journal Supplement Series* **208**.2 (2013), 20. DOI: 10.1088/0067-0049/208/2/20. arXiv: 1212.5225.

[142] Y. Hirata et al. Characterieation of ZSM-5 Zeolite Synthesized from Silica Stone (Ioh Island, Kagoshima Prefecture). *Nippon seramikkusu kyokai gakujutsu ronbunshi* **99**.12 (1991), 1255–1259.

[143] F. Göltl et al. Van Der Waals Interactions between Hydrocarbon Molecules and Zeolites: Periodic Calculations at Different Levels of Theory, from Density Functional Theory to the Random Phase Approximation and Møller-Plesset Perturbation Theory. *The Journal of Chemical Physics* **137**.11 (2012), 114111. DOI: 10.1063/1.4750979.

[144] J. Datka et al. Low Temperature IR Studies of CO Sorbed in ZSM-5 Zeolites. *Journal of Molecular Structure* **511-512** (1999), 133–139.

[145] J. Sárkány. Zeolite Proton-Assisted Reoxidation of Cu0 in over-Exchanged CuII-ZSM-5 Reduced by Hydrogen. (1) Reoxidation in Ar Stream: An FTIR Study. *Physical Chemistry Chemical Physics* **1** (1999), 5251–5257.

[146] E. V. Starokon et al. Oxidation of Methane to Methanol on the Surface of FeZSM-5 Zeolite. *Journal of Catalysis* **300** (2013), 47–54. DOI: `10.1016/j.jcat.2012.12.030`.